HHS Public Access

Author manuscript

Biomacromolecules. Author manuscript; available in PMC 2020 August 03.

Published in final edited form as:

Biomacromolecules. 2018 October 08; 19(10): 4084–4097. doi:10.1021/acs.biomac.8b01088.

Peptide-functionalized hydrogel cubes for active tumor cell targeting

Bing Xue[1,&], **Veronika Kozlovskaya**[1,&], **Mohammad Asif Sherwani**[2], **Sithira Ratnayaka**[1], **Shahriar Habib**[1], **Theron Anderson**[1], **Marina Manuvakhova**[3], **Lidija Klampfer**[3], **Nabiha Yusuf**[2], **Eugenia Kharlampieva**[1,4,*]

[1]Department of Chemistry, University of Alabama at Birmingham, Birmingham, AL, 35294, USA

[2]Department of Dermatology, University of Alabama at Birmingham, Birmingham, AL, 35294, USA

[3]Southern Research, Birmingham, AL, 35205, USA

[4]Center of Nanoscale Materials and Biointegration, University of Alabama at Birmingham, Birmingham, AL, 35294, USA

Abstract

Conjugation of bioactive targeting molecules to nano- or micrometer-sized drug carriers is a pivotal strategy to improve their therapeutic efficiency. Herein, we developed pH- and redox-sensitive hydrogel particles with a surface-conjugated cancer cell targeting ligand for specific tumor-targeting and controlled release of the anticancer drug doxorubicin. The poly(methacrylic acid) (PMAA) hydrogel cubes of 700 nm and 2 μm with a hepsin-targeting (IPLVVPL) surface peptide are produced through multilayer polymer assembly on sacrificial cubical mesoporous cores. The direct peptide conjugation to the disulfide-stabilized hydrogels through a thiol-amine reaction does not compromise the structural integrity, hydrophilicity, stability in serum or the pH/redox sensitivity, but affects the internalization by cancer cells. The cell uptake kinetics and the ultimate extent of internalization is controlled by the cell type and hydrogel size. The peptide modification significantly promotes the uptake of the 700 nm hydrogels by hepsin-positive MCF-7 cells due to ligand-receptor recognition but has a negligible effect on the uptake of 2-μm PMAA hydrogels. The selectivity of 700-nm IPLVVPL-PMAA hydrogel cubes to hepsin-overexpressing tumor cells is further confirmed by a 3- to 10-fold higher particle internalization by hepsin-positive MCF-7 and SK-OV-3 compared to hepsin-negative PC-3 cells. This work provides a facile method to fabricate enhanced tumor-targeting carriers of submicrometer size and improves the general understanding of particle design parameters for targeted drug delivery.

Graphical Abstract

[*]**Corresponding Author:** ekharlam@uab.edu.

[&]B.X. and V.K. contributed equally to this work.

Author Contributions

The manuscript was written through contributions of all authors. All authors have given approval to the final version of the manuscript.

The authors declare no competing financial interest.

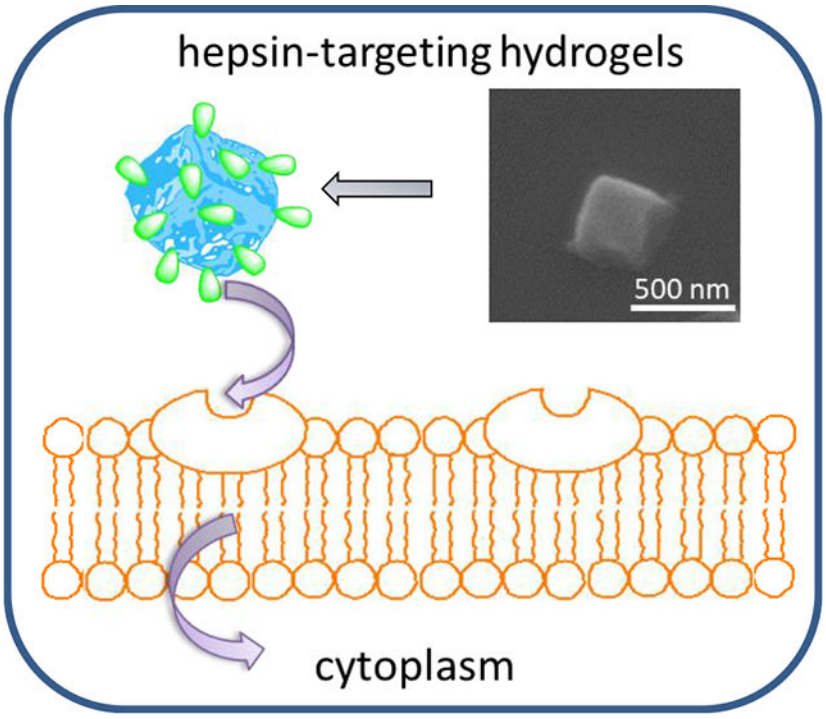

Keywords

poly(methacrylic acid); multilayer hydrogel; hepsin; tumor-targeting; stimuli-responsive; particle size

Introduction

Particle conjugation with bioactive ligands have shown considerable promise for controlled drug delivery due to improved diagnostic and therapeutic outcomes by up-regulating the retention of probes/therapeutics in cancerous tissues.[1] Typically, targeting enhancement is attributed to specific binding affinity between ligands and their corresponding receptors that are over-expressed in the targeted cells.[2–,3,4] Peptides are particularly advantageous due to their high accessibility, ease of chemical modification, good tissue penetration and low immunogenicity.[5,6] The relatively low cost and the ease of upscaling render peptide-decorated particles attractive for clinical applications in tumor targeting treatment.[7,8]

Hepsin is a type II transmembrane serine protease which is overexpressed in many cancer cells, but is absent or found at a low expression level in their non-malignant counterparts.[9] The distinct specificity, appropriate location on the cell membrane and expression enhancement in the early stage of tumor growth make hepsin an ideal target in cancer detection and therapy.[10] However, drug delivery constructs targeting hepsin-overexpressing cancer cells have been underexplored due to the lack of potent and commercially available targeting ligands. Recently, IPLVVPL peptide and its synthetic counterpart have been identified as efficient hepsin-binding ligands that show preferable affinity (190 ± 2.2 nmol/L) to hepsin-positive cells.[10] IPLVVPL-coated iron oxide nanoparticles were explored

for early prostate cancer detection and the nanoparticles showed a 3-fold higher accumulation in hepsin-positive LNCaP tumors compared to the bare nanoparticles *in vivo*.[10] In another study, IPLVVPL-conjugated liposomes displayed 9- to 26- fold higher uptake by hepsin-positive cells compared to non-modified liposomes.[11]

Along with peptide-controlled active targeting, passive tumor targeting based on carrier size has also been investigated.[12] Particle size plays a pivotal role in regulating drug carrier interaction with cells, *in vivo* circulation, and biodistribution[13,14] In this respect, studies on targeting efficacy have been mostly focused on nano-systems (< 500 nm) due to the ease of particle synthesis, favorable cellular uptake, and localization in tumor tissue due to the enhanced permeability and retention (EPR) effect.[14,15] For instance, 50-nm mesoporous silica particles were reported to have the largest internalization by Hela cells among a series of particles in the 30–280 nm size range.[16] Similarly, although drug-loaded micelles ranging from 30 to 100 nm in size showed *in vivo* accumulation in tumor sites, the 30-nm micelles demonstrated extraordinary penetration even into poorly permeable tumors.[17]

In contrast to the particles discussed above, other biologically active entities both natural and synthetic exhibit a wide size distribution over nm to μm scales.[18,19] For example, despite their slightly larger size, the EPR effect was observed for bacteria larger than 1 μm.[20] Micron-sized red blood cells have also been demonstrated as effective bioactive vehicles for targeted drug delivery.[21,22] Synthetic soft PRINT (Particle Replication in Nonwetting Templates) hydrogels ranging from 0.8 to 8.9 μm exhibited longer circulation time when their size approached that of red blood cells, further demonstrating the potential of micron-sized particles for *in vivo* drug delivery.[23] Increasing the size of hydrogel rods from 400 to 800 nm also improved their cellular uptake.[24] The above observations have inspired the development of soft synthetic carriers of sub-micrometer (>500 nm) to micrometer size (1–5 μm) for tumor detection and/or therapy. Importantly, the ability to tune the particle rigidity/elasticity is among the main advantages of polymeric vehicles as drug carriers as it allows for a facile regulation of their biological activity.[25] Thus, decreasing the elastic modulus of polyethylene glycol (PEG) nanogels from 3000 to 10 kPa was shown to increase their *in vivo* circulation up to 2 hours.[26] Prolonged circulation in blood was also observed for micron-sized PRINT hydrogels where the 8-fold lower elastic moduli of the particles led to a 30-fold increase in the elimination half-life.[27] In addition to affecting the circulation time, tuning the elasticity of particles can regulate their association with cancer cells and improve the accumulation in targeted sites.[26] A recent study has demonstrated that softer nanoliposomes (45kPa) are 2.6-fold more efficient in accumulating in 4T1 tumors compared to harder particles (19 MPa), indicating the advantages of reduced elasticity for the tumor targeting ability of particles.[28] While those fundamental associations have been elucidated, research on the effect of particle size (from supra-nano to submicron and micron size) in conjunction with relevant variables such as polymer chemistry, surface modification, and cell type on the targeting ability of the carrier is still in its infancy, possibly due to the challenge of simultaneously fine tuning all these parameters.

In this regard, template-assisted layer-by-layer (LbL) assembly is a powerful approach to meet the requirements regarding particle synthesis.[29,30,31] This method relies on the sequential adsorption of macromolecules on a sacrificial particulate template, which affords

precise control over particle size, shape, and composition, as well as physical and biological properties.[32– 33, 34, 35, 36] Submicron- or micrometer-sized multilayer capsules were successfully internalized by varies cell types.[29,37,38,39] The internalization of μm-sized capsules could be attributed to their elasticity and flexibility which allow for deformation and shape change during the cell uptake process.[38] For example, 3-μm (tannic aicid/poly(N-vinylpyrrolidone)) (TA/PVPON) capsules can pass through 0.8-μm pores, demonstrating their possible extravasation which can be used for passive targeting of tumors.[38] Multilayer microcapsules have also been shown useful for various *in vivo* applications.[40,41]

We have recently developed porous poly(methacrylic acid) (PMAA) multilayer-derived hydrogels of cubical and spherical shapes with pH- and redox-sensitivity which are capable of encapsulation and stimuli-triggered release of hydrophilic doxorubicin and hydrophobic 7-(benzylamino)-3,4-dihydro-pyrrolo[4,3,2-de]quinolin-8(1H)-one (BA-TPQ) anticancer drugs. 42,43,44 Those particles were obtained upon cross-linking of PMAA in PMAA/poly(vinylpyrrolidone) (PVPON) multilayers assembled within mesoporous sacrificial templates. As compared to hollow capsules, these network particles provide much larger surface area due to the polymer network distributed throughout the entire particle volume, which is important for drug loading efficiency and release.[42]

In this work, we report on a facile method to conjugate hepsin-targeting IPLVVPL peptide to pH- and redox-sensitive PMAA hydrogel cubes of tunable size for targeted therapy of hepsin-overexpressing tumors. The surface conjugation of the peptide to the hydrogel matrices is conducted though a thiol-amine reaction. The effects of the particle size and ligand conjugation on hydrogel integrity, morphology, and stimuli-triggered release of doxorubicin is studied. We also explore the influence of cell type and incubation time on internalization of IPLVVP-PMAA hydrogels using the hepsin-positive MCF-7 and SK-OV-3 compared to the hepsin-negative PC-3 cell lines. To the best of our knowledge, this is the first example of hepsin-targeting stimuli-responsive submicron-size drug carries for active tumor targeting. The integration of an active targeting moiety, pH-sensitivity and redox-triggered degradation into the polymeric networks represents a new platform for efficient delivery of therapeutics. In addition, this work has investigated the interplay of particle size, surface ligand modification and cell type on the interaction between hydrogels and cancer cells, which improves the understanding of carrier design in cancer therapy.

Experimental Section (Materials and Methods)

Materials.

Poly(methacrylic acid) (PMAA, average M_w 21,800 g mol^{-1}), poly(N-vinylpyrrolidone) (PVPON, average M_w 10,000 g mol^{-1}), poly(ethylenimine) (PEI, average M_w 25,000 g mol^{-1}), were purchased from Sigma-Aldrich. 1-Ethyl-3-(3-(dimethylamino)propyl)-carbodiimide hydrochloride (EDC) was obtained from Chem-Impex International. Fluorescein isothiocyanate (FITC)-labeled IPLVVPL hepsin-targeting peptide was synthesized by Biomatik in the following configuration: IPLVVPL-PEG-Cys-Lys[FITC] (MW 1515.1 g mol^{-1}). Monobasic sodium phosphate, hydrochloric acid, sodium hydroxide, ethylenediaminetetraacetic acid (EDTA), dimethylformamide (DMF), fluorescein isothiocyanate (FITC) and N-succinimidyl iodoacetate (SIA) were from Fisher Scientific

and used as received. Wheat Germ Agglutinin, Alexa Fluor™ 555 Conjugate (WGA Alexa 555) was purchased from ThermoFisher Scientific. Ultrapure deionized water with a resistivity of 18.2 Ω cm was used in all experiments (Evoqua).

Fabrication of biodegradable PMAA hydrogel particles of different size.

Cubical $MnCO_3$ particles of 2 μm were synthesized as described previously.[43] The submicron $MnCO_3$ cores were prepared as follows. The nano-seed solution was prepared fresh by mixing 0.0081g $MnSO_4$ and 0.0810g NH_4HCO_3 in 400 mL of DI water. The nano-seed solution was poured into 200 mL $MnSO_4$ solution (1.2 g L^{-1} with 0.5% of isopropanol) followed by the addition of 200 mL NH_4HCO_3 solution (4.75 g L^{-1} with 0.5% of isopropanol). The mixture was heated for 12 min at 80 °C and the particles were separated by filtration through 0.45-μm pore cellulose acetate filters (Whatman). $MnCO_3$ particles of 700 nm and 2 μm were heated at 700 °C for 3 h, yielding porous Mn_2O_3 for polymer deposition. The cubical PMAA hydrogels were then prepared using multilayer deposition of PVPON and PMAA as described previously.[42] Briefly, porous Mn_2O_3 template particles were vortexed in aqueous PEI solution for 1 h to render particle surfaces cationic followed by sequentially depositing PMAA and PVPON from 1.5 mg mL^{-1} polymer solutions (pH = 3.6, 0.01 M phosphate) to obtain a $(PMAA/PVPON)_5$ multilayer. Each polymer adsorption step included 15-min sonication (Branson ultrasound bath) followed by 30-min shaking (1000 rpm). After each deposition step, particles were rinsed twice with 0.01 M phosphate buffer (pH = 3.6) to remove non-adsorbed polymer. Porous core dissolution was carried out by exposure of the core-shell templates to 6 M HCl for 24 h followed by six rinses with DI water at pH = 2. The chemical cross-linking of polymeric particles was performed through conjugation of amine and carboxylic groups. Carboxylic groups of PMAA layers were first activated with EDC (5 mg mL^{-1}, pH = 5, 0.01 M phosphate) for 40 min. The polymeric particles were then incubated with cystamine hydrochloride (2 mg mL^{-1}, pH = 5.8, 0.01 M phosphate) for 24 h under shaking. PVPON was released from the PMAA networks at pH = 8 (0.01 M phosphate) for 24 h followed by EDTA treatment (pH = 7, 0.1 M) for 3 h. The purified PMAA multilayer hydrogel particles were dialyzed against DI water for 3 days (Float-a-Lyzer MWCO = 20 kDa, Spectrum Labs).

Conjugation of IPLVVPL-PEG-Cys-Lys[FITC] and FITC to PMAA hydrogel particles.

IPLVVPL-modified hydrogel particles (IPLVVPL-PMAA hydrogels) were prepared via a thiol-amine reaction. For that, N-succinimidyl iodoacetate (SIA, 5 mg) was first dissolved in 50 μL DMF followed by dropping into 1.95 mL of 0.01 M phosphate buffer at pH = 8. The final concentration of SIA solution was achieved as 2.5 mg mL^{-1}. PMAA hydrogels were suspended in the SIA solution and shaken for 2 h. Before the conjugation of IPLVVPL-mini-PEG-CK-FITC, the PMAA hydrogels were rinsed twice with 0.01 M phosphate buffer at pH = 8. The peptide solution (0.15 mg mL^{-1}, pH = 6.8) was then mixed with SIA-activated hydrogel particles. The reaction was allowed to proceed at room temperature for 24 h. For visualization of PMAA hydrogel particles using optical microscopy, peptide-free PMAA hydrogels were fluorescently labelled with FITC by mixing PMAA hydrogels with FITC solution (0.1 mg mL^{-1}, pH = 9) for 24 h under shaking. The purification of peptide-conjugated and peptide-free FITC-labeled hydrogel particles was carried out by rinsing with 0.01 M phosphate buffer using centrifugation/re-dispersion until no free FITC was detected

in supernatant UV-vis measurements. The amount of IPLVVPL-PEG-Cys-Lys[FITC] molecules attached to the PMAA hydrogels was determined via a FITC calibration curve (λ = 496 nm) using UV-Vis spectroscopy. The amount of conjugated peptide can be obtained as moles of conjugated peptide per mass (*mg*) of hydrogels. The mass of the attached peptide was determined by subtracting the mass in the supernatant from the mass of the peptide in the initial solution using a peptide calibration curve. The number of peptides per hydrogel can be calculated as follows: the number of peptide per particle $= \frac{moles\ \ of\ \ attched\ \ peptides \times Avogadro's\ \ number}{number\ \ of\ \ particles}$, where the number of particles was counted with hemacytometer.

Scanning Electron Microscopy.

The size, shape and morphology of Mn_2O_3 inorganic particles, PMAA hydrogels and IPLVVPL-PMAA hydrogels were examined with a FEI Quanta™ FEG SEM microscope at 10 kV. A drop of particle suspension was added to a silicon wafer chip (5 mm × 5 mm) and dried overnight at room temperature. The dried specimens were sputter-coated with 5-nm thick silver layer using a Denton sputter-coater.

Confocal Laser Scanning Microscopy (CLSM).

Confocal images of IPLVVPL-PMAA, and doxorubicin (DOX)-loaded DOX-IPLVVPL-PMAA hydrogels before and after serum treatment were obtained with an Nikon A1R+ confocal laser microscope equipped with a 100× oil immersion objective. For serum treatment, the hydrogels were incubated for 24 h at 37 °C with 10% FBS-containing PBS buffer solution (HyClone, 1x). A drop of each hydrogel suspension was added to a Lab-Tek chambered coverglass filled with PBS (pH = 7.4). The hydrogels were allowed to settle at the bottom of the chamber and the fluorescent images were collected using TRITC/FITC filter set to visualize DOX and/or FITC fluorescence within the hydrogel particles.

Turbidity measurements.

Integrity of PMAA hydrogels in the presence of IPLVVPL-PEG-Cys-Lys[FITC] before and after SIA treatment, and the glutathione-induced degradation of IPLVVPL-PMAA hydrogels were studied via turbidity measurements using fluorometry (Varian, Cary Eclipse) at λ=700 nm. The relative solution turbidity was calculated as the ratio of scattering intensity of the hydrogel solution at pre-determined time points to that of the initial non-degraded hydrogel. For the particle integrity study, PMAA hydrogels ($2–3\times10^5$ hydrogels μL^{-1}) or SIA-modified PMAA hydrogels were incubated in IPLVVPL-PEG-Cys-Lys[FITC] solution (0.15 mg mL^{-1}, pH = 6.8) at room temperature for 24 h. The glutathione-induced degradation of IPLVVPL-PMAA hydrogel was carried out by incubation of the hydrogel particles (1×10^5 hydrogels μL^{-1}) with 5 mM glutathione in 1x PBS (HyClone, pH = 7.4, 37 °C).

Synthesis of IPLVVPL-PMAA hydrogel planar films.

The PMAA hydrogel film was prepared as described for the PMAA hydrogel particles above. Briefly, hydrogen-bonded $(PVPON/PMAA)_5$ (the subscript denotes the number of deposited bilayers) multilayer was built up on a Si wafer primed with poly(glycidyl methacrylate) (PGMA)-PMAA bilayer as reported previously.[45] The polymers were

adsorbed from 0.5 mg mL^{-1} polymer solutions in 0.01 M phosphate buffer (pH = 3.6) with the polymer deposition time of 15 min. The crosslinking was carried out by exposure of the film to EDC solution (5 mg mL^{-1}, 0.01 M phosphate) at pH = 5 for 40 min followed by interaction with cystamine (2 mg mL^{-1}, 0.01 M phosphate) at pH = 5.8 for 3 h. The peptide conjugation to the PMAA hydrogel film was done as described for the PMAA hydrogel particles.

Contact Angle Measurements.

Wetting of the peptide-free PMAA and IPLVVP-PMAA hydrogel film surfaces was analyzed by measuring contact angles with a ThetaLite 101 tensiometer (Biolin Scientific). A water droplet (7 μL) was placed on the hydrogel films at room temperature. An average contact angle for each film was obtained from five different spot measurements on film surfaces.

Encapsulation and *in vitro* release of DOX.

DOX was encapsulated into peptide-conjugated hydrogels by incubating the IPLVVP-PMAA particles in 0.2 mg mL^{-1} DOX solution (pH = 6.4, 0.01 M phosphate) for 24 h. The free DOX was rinsed off with 0.01 M phosphate solution at pH = 7.4 five times. The DOX loading per IPLVVP-PMAA hydrogel particle was determined using a DOX calibration curve and calculated as follows: DOX loading = $[(DOX)_i\text{-}(DOX)_s]$/number of hydrogels, where $(DOX)_i$ is the initial amount of DOX and $(DOX)_s$ is the amount of DOX in the supernatant after loading. The number of hydrogel particles was counted under a microscope with a 40x objective using a hemacytometer (Fisher Scientific).

The DOX release from IPLVVPL-PMAA hydrogels was studied at various pH and temperature conditions. DOX-loaded IPLVVPL-PMAA hydrogel suspension (2 mL) in 0.01 M phosphate buffers at pH = 5, pH = 7.4, and pH = 7.4 in the presence of 5mM GSH was incubated under shaking (80 rpm) in a water bath at 37 °C. After the predetermined time intervals, the particles were separated by centrifugation (5 min, 8000 rpm) from solution and the supernatant (1.5 mL) was analyzed by UV-vis spectroscopy (Varian Cary 50). Fresh buffer solution (1.5 mL) was added to maintain the 2-mL total volume.

Cell studies.

MCF-7 cell line (human breast carcinoma cells) was grown in DMEM (Dulbecco's Modified Eagle's Medium; Corning), while SK-OV-3 (human ovarian carcinoma cells) and PC-3 (human prostate carcinoma cells) were cultured in RPMI-1640 (HyClone). All media were supplemented with 10% (v/v) FBS (HyClone), and 1% (v/v) penicilin G (Corning).

Cell viability assay.

MTT assay was used to assess the cytocompatibility of IPLVVPL-PMAA hydrogels. For that, MCF-7 cells were plated in 96-well plates in 100 μL of DMEM supplemented with 10% FBS (HyClone). Following 24 h incubation, 50 μL were removed from each well. Then 50 μL of DMEM with 10% FBS containing 2 μm PMAA or IPLVVPL-PMAA hydrogels (the hydrogel-to-cell ratio was 100) were added to each well with 24-, 48-, and 72-h incubation. The untreated cells were used as control, which underwent incubation under the

same condition. After a certain time interval, 10 μL of MTT solution (5 mg mL^{-1}, Sigma-Aldrich) was added to each well and the plate was incubated for another 4 h. The supernatant was removed, and 100 μL of DMSO was applied to dissolve the formazan. Absorbance was determined at 570 nm using an EnVision microplate reader (PerkinElmer). The experiments were performed in triplicate and the cell viability was expressed as survival percentages of the growth control group. The Student's t-test was applied to assess the statistical significance of each data set.

Cell imaging with CLSM.

MCF-7, SK-OV-3 and PC-3 cells were seeded in a Lab-Tek chambered coverglass with a density of 5×10^4 cells per well. Cells were allowed to adhere for 24 h followed by culturing with IPLVVPL-PMAA or peptide-free PMAA hydrogels at 37 °C in a humidified 5% CO_2 incubator. After 3-h incubation, liquid medium was aspirated, and the cells were washed three times with cold DPBS and covered to a depth of 2–3 mm with 4% paraformaldehyde diluted in 1x PBS for 15 min at room temperature. Fixative was aspirated, and cells were rinsed three times with DPBS for 5 min each. Cell membranes were stained with WGA-Alexa 555 (0.5 μg mL^{-1}, Molecular Probes) for 20 min on ice. Cell nuclei were stained with DAPI (2 μg mL^{-1}, Invitrogen).

Flow Cytometry.

MCF-7, SK-OV-3 and PC-3 cells were seeded at a density of 2.5×10^5 cells per well in a 12-well plate (Corning) and treated with 15 μg mL^{-1} IPLVVPL-PMAA or peptide-free FITC-labeled PMAA hydrogels. Following 1-, 3-, 6- and 24 h incubation, cells were washed three times with cold DPBS, trypsinized and collected by centrifugation at 300 g for 5 min with the concentration of 1×10^6 cells per 300 μL and kept on ice. After that, 50,000 fluorescent events were collected using BD FACS Calibur™ flow cytometer and analyzed by FlowJo. The experiments were performed 4 times for each sample and data were expressed as the mean ± standard deviation. Student t-test was applied to assess the statistical significance of each data set.

Results and Discussion

Synthesis and characterization of peptide-conjugated PMAA hydrogels

Cubical PMAA hydrogels of 2 μm in size were obtained through sequential infiltration of PMAA and PVPON within mesoporous 2.0 ± 0.2 μm Mn_2O_3 templates followed by template dissolution and PMAA chemical cross-linking, according to our previous work.[43] To obtain submicron hydrogels, 0.70 ± 0.05 μm cubical Mn_2O_3 particles were used which were produced by controlling the amount of reagents and heating time (see Experimental). SEM analysis shows that both types of Mn_2O_3 templates exhibit well-defined cubical geometry and uniform porous morphology (Fig. 1a and b). Sequential infiltration of PMAA and PVPON inside PEI-coated Mn_2O_3 templates of both sizes yielded the hydrogen (H)-bonded multilayers throughout both template volumes. After template dissolution, PMAA was cross-linked with cystamine followed by PVPON release, which enabled formation of the corresponding hydrogels of 2.5 ± 0.2 μm and 0.9 ± 0.2 μm at pH=7.4. As demonstrated earlier, the crosslink density of these hydrogels can be controlled by adjusting cross-linking

time and the cross-linker concentration.[42,43] In the dry state, both hydrogels shrank in size to half of their hydrated states resulting in 1.00 ± 0.05 μm and 0.43 ± 0.03 μm particles, respectively, as measured with SEM due to the collapsed polymer chains upon network dehydration (Fig. 1c, d). Both types of hydrogels maintain their cubical geometry in dry state with clearly observed edges and corners, which is consistent with our previous results on 2- and 4-μm PMAA hydrogel particles.[43]

Conjugation of hepsin-targeting Ile-Pro-Leu-Val-Val-Pro-Leu (IPLVVPL) peptide to the hydrogel matrices was conducted through a thiol-amine reaction using free amine groups remaining from single-end attachment of cystamine during PMAA cross-linking. As shown in Scheme 1, the primary amines of the hydrogels reacted with heterobifunctional succinimidyl iodoacetate (SIA) yielding active iodoacetyl groups capable of interacting with the sulfhydryl groups of cysteine in IPLVVPL-PEG-Cyc-Lys[FITC]. The IPLVVPL-PMAA hydrogels were rinsed with pH=7.4 buffer to remove non-bound peptide. After modification with the peptide, the hydrogel particles became yellow-colored due to the FITC moiety on the peptide ligand (Fig. 2a). The CLSM images of the 2-μm IPLVVPL-PMAA hydrogel particles revealed a bright and uniform green fluorescence throughout the entire particle volume, indicating successful peptide conjugation to the PMAA network (Fig. 2b).

As determined by UV-vis spectroscopy, the amount of the peptide attached to the hydrogel particles were 15.9 ± 2 and 14.5 ± 1.4 nmol mg^{-1} for 700 nm and 2 μm PMAA hydrogels, respectively. These values are not statistically different indicating that the peptide conjugation to the hydrogel particles is not dependent on the particle size. Likewise, 700-nm and 2-μm peptide-modified hydrogels showed similar surface charges at pH = 7.4 with the ζ-potential values of −17.8 ± 0.6 mV and −18.9 ± 0.7 mV, respectively, suggesting a similar amount of the peptide conjugated to the particle surfaces. Previous studies have demonstrated that variation of surface charge can significantly alter particle-cell interactions, specifically, the attachment of particles to the cellular membrane as well as internalization kinetics.[14,46] Thus, the fact that 700-nm and 2-μm PMAA hydrogels have similar surface charges is important for further analyses of their interactions with cancer cells. In addition, the negative surface charge of these hydrogels can be advantageous for *in vivo* use since anionic particles were found to have lower systematic immune response and cytotoxicity.[47,48]

One of the most appealing features of cystamine-crosslinked PMAA hydrogels is the redox sensitivity arising from the disulfide bonds created during crosslinking that leads to particle biodegradation and fast drug release.[7,44] However, the thiol-disulfide exchange between the cysteine residues from the peptide molecules and the disulfide bonds in the PMAA hydrogels may occur as a side reaction during the conjugation process, which could compromise the 3-dimensional structure of these hydrogels. SEM analysis revealed that the hydrogels retained their 3-dimensional structure with distinguishable corners and faces after the peptide-conjugation (Fig. 2c–f). The sizes of dry IPLVVPL-PMAA hydrogels were found to be 0.42 ± 0.05 and 1.00 ± 0.05 μm after the peptide-modification of 0.7 and 2 μm hydrogels particles, respectively, which are very close to their corresponding dimensions before modification (0.43 ± 0.03 μm and 1.00 ± 0.05 μm). Thus, the peptide-conjugation

affected neither the structural integrity of the hydrogel particles nor their size or shape (Fig. 1c,d).

The chemical stability of PMAA hydrogels in the presence of the thiol groups of the peptide ligand was assessed by turbidity analysis of the PMAA hydrogel suspensions in the presence of IPLVVPL-PEG-Cyc-Lys[FITC]. Direct incubation of the PMAA hydrogels with the peptide ligand resulted in decreased suspension turbidity from 100 to 8% indicating PMAA network degradation (Fig. 3a). This result suggests that the thiol end groups in the ligand are able to reduce the disulfide bonds in the PMAA network causing its dissolution. In contrast, when the PMAA network was allowed to react with SIA first, the turbidity of the PMAA hydrogel suspension did not decrease below 100% throughout the 24 h incubation (Fig. 3a), indicating the chemical stability of the network in the presence of the peptide ligand. This observation can be explained by the high reactivity of the iodoacetyl groups toward thiols resulting in hindered exchange between -SH end groups of the ligand and -S-S- links of the hydrogel. In addition, the IPLVVPL-PMAA hydrogel particles maintained their shape and size at pH=7.4 (0.01 M phosphate) for 6 months at room temperature, suggesting their long-term stability in solutions.

Wettability of the dry hydrogel films before and after peptide conjugation was analyzed using contact angle measurements. The peptide-free PMAA hydrogel film shows a contact angle of $\theta = 48 \pm 1°$, which is higher than the previously reported contact angle $\theta < 10°$ for ethylenediamine (EDA)-cross-linked PMAA hydrogel films.[49] The increased hydrophobicity of cystamine-cross-linked PMAA film as compared to their EDA-crosslinked counterparts is due to the relatively hydrophobic nature of cystamine compared to EDA.[42] After peptide conjugation, the contact angle was measured as $49 \pm 2°$ (Fig. 3b) which was similar to that of the unmodified hydrogel film, indicating that the peptide surface modification had a negligible effect on the hydrogel surface wettability.

The result suggests that peptide molecules may comprise a relatively small portion of the network and do not significantly alter the hydrophilicity of the hydrogel. Thus, both the peptide-conjugated and peptide-free PMAA hydrogels are hydrophilic with contact angles less than 90°.[50] The hydrophilicity of the peptide-modified hydrogels is also evidenced by their dramatic volume change upon hydration due to the hydrophilic ionizable carboxylic groups. The 2.5 ± 0.2 μm hydrogels swell up to 15.6-fold their original volume at pH = 7.4 (0.01 M phosphate) compared to their size of 1.00 ± 0.05 μm in the dry state. This inherent hydrophilicity can be helpful in reducing non-specific protein adsorption and improving biocompatibility of the PMAA hydrogel cubes.[51] These results indicate that ligand conjugation to the disulfide-stabilized PMAA hydrogels through a thiol-amine reaction does not compromise their structural integrity, morphology, or hydrophilicity, demonstrating a facile synthetic strategy that could be applied for modifying disulfide-stabilized drug carriers with bioactive agents.

Hydrogel degradation and drug release

We found earlier that cystamine-crosslinked PMAA hydrogels dissociated in the presence of intracellular 5 mM glutathione (GSH), a tripeptide enzyme capable of reducing disulfide bonds to the corresponding thiols in cells.[42] We investigated the redox-induced degradation

of the 2-μm IPLVVPL-PMAA hydrogels due to reduction of the disulfide links in the PMAA network by analyzing the turbidity of the hydrogel particle solutions before and after the peptide-attachment using fluorometry. The turbidity of the IPLVVPL-PMAA hydrogel solution did not change during 6 h incubation at pH = 7.4 (0.01 M phosphate) indicating their stability at physiological conditions (Fig. 4a). In contrast, the IPLVVPL-PMAA hydrogel solution showed decreased turbidity after only 10 min in the presence of 5 mM GSH, and became completely transparent in 5 hours with only 1.0 ± 0.8% turbidity measured in solution (Fig. 4a). In comparison, the peptide-free PMAA hydrogel particles degraded faster than the IPLVVPL-PMAA hydrogels, with a relative turbidity of 28 ± 2% after 1 h incubation in the GSH solution, compared to that of 54 ± 2% for the IPLVVPL-PMAA particle solution. The complete degradation of the peptide-free PMAA hydrogel particles occurred after 2-h incubation in GSH resulting in the residual relative turbidity of 2 ± 1% (Fig. 4a). Evidently, the peptide modification slowed down the diffusion of GSH inside the particles, similarly to the slowed GSH-induced degradation of the PMAA hydrogel cubes with encapsulated hydrophobic BA-TPQ anticancer drug reported in our previous work.[44]

The peptide-PMAA hydrogel particles were also loaded with the anticancer drug doxorubicin (DOX) and the drug release from the IPLVVPL-PMAA hydrogels was studied. The loading capacity was measured as $(7.32 \pm 2.8)\times10^{-4}$ ng per hydrogel particle by UV-vis spectroscopy. The DOX loading was similar to that of peptide-free PMAA hydrogels, $(6.8 \pm 0.8) \times10^{-4}$ ng per hydrogel particle,[42] which indicated that the IPLVVPL conjugation did not affect the ionic interaction between DOX and the hydrogel network. DOX release from the particles was analyzed at pH=7.4 in the presence or absence of GSH, and at pH=5.0 which mimics the intracellular lysosome environment.

The cumulative DOX release was 23 ± 4% and 58 ± 4% at pH = 7.4 and pH = 5, respectively, after 24 h incubation at 37 °C, indicating slow drug release at physiological pH (Fig. 4b). The faster DOX release at lower pH is due to the lower degree of ionization of the carboxyl groups in acidic conditions that weakens the interaction between DOX and the hydrogels. In contrast to these results, the presence of 5 mM GSH at pH=7.4 significantly increased DOX release to 97 ± 1% after 24 h incubation due to the dissolution of the hydrogel because of the disulfide cleavage (Fig. 4b). The above results suggest that the majority of DOX releases at pH = 7.4 when the network is dissociated in the presence of GSH, which correlates with previous reports from others where decreasing solution pH or elevating the concentration of a reducing agent can enhance the drug release.[52–,53,54] In addition, dissociation of the hydrogel particles to PMAA molecules with M_w ~ 21 kDa can minimize their systemic toxicity as they can be easily excreted via the kidneys.[54,55]

Although biocompatibility of PMAA hydrogel capsules crosslinked with disulfide linkages has been demonstrated in non-malignant cells earlier,[56] the cytotoxicity of the peptide-conjugated PMAA hydrogels was evaluated in this work using an MTT assay. Both the peptide-free and peptide-conjugated hydrogels were non-toxic to MCF-7 cells with the cell viability above 95% after 72 h incubation with the hydrogel particles (Fig. 4c). The data indicates that the conjugation of the peptide molecule into the network did not induce toxicity to cells. The results are also in agreement with the reported improved

cytocompatibility of PMAA-containing nanogels and hydrogel capsules,[57,74] as compared to other LbL polyelectrolyte capsules (e.g. alginate/polylysine) which showed cytotoxicity.[37]

We evaluated the colloidal stability of 2-μm DOX-loaded IPLVVPL-PMAA hydrogel particles *in vitro* by incubating the particles in PBS solution containing 10% FBS at 37 °C for 24 h followed by visualization with confocal microscopy (Fig. 5).

Before serum addition, the bright red fluorescence from DOX was found to co-localize with the green FITC fluorescence that was used to visualize the PMAA network, which indicated that DOX was uniformly distributed throughout the particle volume (Fig. 5, left column). After 24 h incubation in serum, the DOX-loaded IPLVVPL-PMAA hydrogel particles retained the strong red fluorescence (DOX) which suggested the excellent capability of the hydrogel particles for DOX retention. Moreover, the serum exposure did not lead to particle aggregation, due to the hydrophilicity of the particles.[58] This result correlates well with an earlier report where PMAA hydrogel capsules had a low level of interaction with serum.[56] In addition, the presence of 2-mer PEG segments in the peptide ligand used for PMAA hydrogel conjugation may also be advantageous in impeding the hydrogel-serum interaction due to the well-known low-fouling nature of PEG.[59, 60]

Effect of particle size on interaction of peptide-free PMAA hydrogel particles with MCF-7 cells

To evaluate the *in vitro* interactions of the PMAA hydrogel cubes with cells, 700 nm and 2 μm peptide-free and IPLVVPL-PMAA hydrogels were incubated with hepsin-positive MCF-7 cells for various time periods. We found that even without a targeting ligand, the PMAA particles of both sizes were moderately internalized by the MCF-7 cells. The CLSM images in Figure 6 demonstrate that while many 2-μm PMAA hydrogels were attached to the cell surface (the cell membrane is labeled with red fluorescence) after 3 hours of incubation, fewer 700 nm hydrogels can be observed in the vicinity of the cell membranes (Fig. 6a, b) after that time. However, the 700 nm PMAA hydrogel internalization became more pronounced after 24 h incubation with the cells, although to a lesser extent than that in the case of larger 2-μm PMAA hydrogels (Fig. 6c, d).

Internalization of the hydrogels by MCF-7 cells after 1, 3, 6 and 24 hours of incubation was quantified using flow cytometry (Fig. 6e). The internalization kinetics showed that the cellular uptake was dependent on both particle size and the incubation time. The percentage of cells with internalized 700 nm hydrogels consistently increased from 3.8 ± 0.9 % to 14.2 ± 0.9 % ($p<0.01$), to 25 ± 2 % ($p<0.05$), and to 34 ± 6 % in 1, 3, 6, and 24 hours, respectively. In contrast, 2 μm particles showed a two-fold increase in the cellular uptake from 22 ± 5 to 46 ± 3% in 1 and 3 hours respectively, followed by no changes in particle-cell interactions for longer incubation times, which could be due to the early occurrence of saturation in cellular internalization. The latter result correlates with the previous work on cell internalization of 2 – 5 μm cubical PRINT particles by HeLa cells that reached a plateau within 1 h of incubation.[61] In a relevant example, the cellular uptake kinetics of shaped hydrogel discs and rods in different cell lines indicated a time-dependent manner of cellular

internalization over 20–80 hours.[24] The reported observations suggest that the kinetics of cell-particle interaction is contingent upon the particle properties and cell type.

The micrometer-sized hydrogel uptake is mostly due to micropinocytosis and/or phagocytosis, which are non-specific mechanisms for cellular internalization.[62–,63,64] The previous works have applied different pharmaceutical/chemical inhibitors interfering the internalization pathways to understand the mechanisms of cellular uptake of 2–4 μm (poly-(sodium 4-styrene sulfonate)/poly-(allylamine hydrocholoride)) PSS/PAH capsules.[64] The results indicated that addition of methyl-beta-cyclodextrin (interfering macropinocytosis) and bafilomycin A_1 (interfering phagocytosis) significantly decreased particles internalization by MDA-MB-231 breast cancer cells with 93% and 84% of inhibition, respectively.[64] In contrast, chlorpromazine, dynasore, potassium depletion and nystatin treated groups only showed 17% to 0% inhibition of capsule uptake, indicating the clathrin- and caveolae-endocytosis were not dominant in 2–4 μm capsule internalization.[64] A study on more rigid polystyrene particles (3 μm) showed cytochalasin D (phagocytosis inhibitor) could completely inhibit particle internalization by SKBR-3 breast cancer cells while dynasore did not affect uptake of particles.[65] Therefore, micropinocytosis and/or phagocytosis can be considered the main mechanisms responsible for the internalization of 2 μm PMAA hydrogels by MCF-7 breast cancer cells. Despite that uptake of particle larger than 1 μm can be facilitated by macropinocytosis[66] and 2–3 μm particles have better phagocytosis rate[67], these two mechanisms also contribute to the cell internalization of supranano particles (>500 nm).[24,32,62,63] In addition, a clathrin-dependent endocytic mechanism might also be involved in the cellular uptake of 700-nm PMAA hydrogels. The clathrin-mediated endocytosis was reported to be mainly responsible for the internalization of macromolecules or small particles,[68] however, several studies found that this mechanism was also predominant in the internalization of particles larger than 500 nm. For instance, Zelikin *et al.* found that soft PMAA capsules with sizes ranging from 300 nm to 1 μm can be internalized by cells through a clathrin-mediated pathway.[69] Likewise, 1-μm PRINT particles internalization was explained through clathrin-mediated endocytosis where about 80% of cell uptake inhibition was observed upon chlorpromazine addition.[61,70] Thus, we suggest that clathrin-mediated endocytosis along with micropinocytosis/phagocytosis are involved in the cellular uptake of 700-nm hydrogel cubes; while micropinocytosis/phagocytosis are mainly responsible for the internalization of 2-μm PMAA hydrogels.

Another observation is that the uptake of 2-μm PMAA hydrogels is significantly enhanced compared to their smaller 700-nm counterparts at each time point (Fig.6e; $p < 0.01$ for 1, 3 and 6 h, and $p < 0.05$ for 24 h). The greater internalization extent of the larger PMAA hydrogel particles indicates their amplified association with the cells at the early time of incubation. Indeed, a particle binding to the cell surface was found imperative to initiate the cellular uptake of particles regardless of internalization mechanisms.[29,71] In this regard, an increase in the particle size could improve the non-specific binding to the cells as a result of the larger contact area between the particle surface and cell membrane.[29] The difference in the particle sedimentation is another important factor influencing cell internalization.[24] A faster sedimentation of 2 μm PMAA hydrogels can generate a high particle concentration near the cell membrane in a shorter time which promotes binding and internalization.

Similar results have been observed in the cellular uptake of hydrogel discs and rods with larger particles being internalized more efficiently.[24]

In this work, the hydrogel particle size variation is the main factor that leads to the difference in the internalization kinetics since both larger and smaller of hydrogels have the same chemical composition and shape. The cell-binding enhancement and sedimentation acceleration induced by the increase in the particle size results in faster internalization of larger PMAA hydrogels due to non-specific interactions with the cell membrane. Thus, for the peptide-free PMAA particles, their non-specific internalization is mainly controlled by the particle size in which the increase in size not only improves the extent of cellular uptake but also increases the speed of internalization.

Effect of particle size on interactions of IPLVVPL-PMAA hydrogels with MCF-7 cells

To investigate the effect of the peptide-modified IPLVVPL-PMAA particle size on cellular uptake, hepsin-positive MCF-7 cells were cultured with 2 μm and 700 nm IPLVVPL-PMAA hydrogel cubes. The CLSM images of the cells incubated with the IPLVVPL-PMAA particles demonstrate that a moderate uptake by the cells of the larger hydrogel particles did not significantly change after incubation time was increased from 3 to 24 h (Fig. 7a, b), however, the extent of the particle internalization by the cells dramatically increased in the case of the smaller 700 nm IPLVVPL-PMAA particles (Fig. 7c, d). The flow cytometry analysis of the cells incubated with the particles demonstrate that 700 nm IPLVVPL-PMAA uptake consistently progressed from 9 ± 2% to 67 ± 6% as incubation time increased from 1 to 24 h (Fig. 7e). In contrast, the percentage of cells that internalized 2 μm IPLVVPL-PMAA hydrogels remains mostly unchanged between 25% and 30% during 24 h incubation with virtually no effect of the incubation time on cellular uptake of the large particles. Importantly, the uptake of 700 nm IPLVVPL-PMAA hydrogels is 2.5-fold higher ($p<0.05$) than that of their 2 μm counterparts after 24 h (Fig.7e). Another observation is that the uptake of 700 nm IPLVVPL-PMAA is ~2-fold higher than the corresponding peptide-free PMAA hydrogels at 3, 6 and 24 h ($p<0.05$) (Fig. 6e). The 2 μm IPLVVPL-PMAA particles exhibit an opposite trend and undergo suppressed uptake as compared to peptide-free PMAA hydrogels. Thus, for example, the population of cells with internalized 2 μm IPLVVPL-PMAA hydrogels was 25±1% and 27±1% after 1- and 24 h incubation, respectively, for IPLVVPL-PMAA, while it was 22±5% and 46±3% after 1 and 24 h incubation, respectively, for PMAA (Fig. 6e and 7e). Therefore, 700 nm IPLVVPL-PMAA hydrogel particles are internalized much more efficiently with ~3-fold higher uptake than their larger counterparts, unlike PMAA hydrogels whose uptake decreased for smaller particles (Fig.6). At the same time, 700 nm IPLVVPL-PMAA show ~2-fold greater internalization than PMAA particles of the same size, but their larger counterparts exhibit an opposite trend.

The aforementioned results suggest that the size of particles plays an important role in regulating their active-targeting ability. Specifically, the targeting function of IPLVVPL is found to be more effective in the submicron PMAA hydrogels. The high affinity of the peptide to hepsin promotes the attachment of 700 nm IPLVVPL-hydrogels to the hepsin-overexpressing cells followed by their uptake, which is more much more efficient than the non-specific internalization of the 700 nm peptide-free PMAA hydrogels. The peptide-

mediated selectivity to submicron carriers was observed previously when IPLVVPL-decorated liposomes and iron oxide nanoparticles showed improved targeting capability to hepsin-overexpressing cells.[10,11] Our results also show that active targeting ability is suppressed in the case of the 2 μm particles which indicates different mechanisms for the IPLVVPL-PMAA hydrogels of different sizes. As reported previously, an increase in size from nanoscale to microscale compromised tumor selectivity of A33 antigen-coated particles due to the increased non-specific binding.[29] For instance, RGD-functionalized chitosan (CHI)/elastin-like recombinamers (ELRs) microcapsules of 3~4 μm have demonstrated similar internalization efficiency compared to the non-modified capsules, indicating that the RGD-conjugation was not prominent in the cellular uptake.[62] Likewise, 500 nm PMAA capsules had a better specific association to the targeted cell lines compared to the larger particles.[29]

The different internalization behavior of PMAA hydrogels observed here can be attributed to the fact that the decrease in the particle size decreases the non-specific binding of the hydrogel to the cell membrane, which, in turn, highlights the effect of the peptide-mediated specific affinity to the targeted cells. Unlike small peptide-free PMAA particles, whose non-specific internalization increases with increasing particle size, in the small peptide-conjugated IPLVVPL-PMAA particles, the targeting ability of the peptide prevails over the non-specific interactions resulting in a greater extent of internalized IPLVVPL-PMAA than PMAA. Indeed, the non-specific micropinocytosis should be predominant in the cellular uptake of 2 μm particles after the peptide conjugation, while ligand-mediated specific-endocytosis plays an important role in cell internalization of small 700 nm hydrogels. Thus, the relatively larger size of PMAA hydrogels promotes their non-specific binding; however, it also weakens their tumor targeting ability. The phenomenon can be attributed to the stronger initial attachment of the 2 μm IPLVVPL-PMAA hydrogel cubes to the cellular membrane due their larger surface area, followed by their suppressed internalization.

The explanation is consistent with a recent work of DeSimone and colleagues who controlled the PRINT hydrogel-cell binding by tuning the targeting ligand density on the hydrogels to study how the binding affinity would affect the cellular uptake of PRINT particles.[72] Their results indicated that an increase in the ligand density could first facilitate particle association with the cell membrane, which improved cell internalization; however, further increasing the ligand density beyond the optimal value led to a higher surface attachment but lower internalization of the PRINT hydrogels.[72] This suggests the crucial role of optimal surface affinity to improve the cellular uptake of particles. Thermodynamic models also indicated that the cellular uptake could be inhibited due to the adhesion strength induced by a higher ligand density.[73] Therefore, the decrease in the cellular internalization of 2 μm peptide-modified PMAA hydrogels observed in this work can be attributed to the strengthened adhesion of the hydrogels to the cell membrane caused by the combination of enhanced non-specific binding and ligand-receptor activated specific binding.

Interaction of 700-nm IPLVVPL-PMAA hydrogels with MCF-7, PC-3 and SK-OV-3 cells

To confirm the targeting ability of 700-nm IPLVVPL-PMAA hydrogel particles and study the effect of the cell type on the hydrogel internalization, the interactions between the

IPLVVPL-PMAA hydrogels and hepsin-positive (+) MCF-7 and SK-OV-3, and hepsin-negative (−) PC-3 cancer cells were explored. Representative images of the cells incubated with the peptide-conjugated 700 nm IPLVVPL-PMAA particles are shown in Figure 8a–c. The IPLVVPL-PMAA hydrogels are strongly associated with the hepsin-positive MCF-7 and SK-OV-3 cells after 3 h incubation. In addition, some of the hydrogel particles undergo an intracellular degradation after internalization, which can be seen as a blurring of the green fluorescence signal in the cell plasma (Fig. 8a–c). The intracellular particle degradation occurs due to the redox-sensitivity of the IPLVVPL-PMAA hydrogels. A similar phenomenon was observed with biodegradable thiolated-PMAA spherical capsules, where the fluorescent dye released from the capsules was blurred in the cytoplasm, while the fluorescence signal from a non-degraded capsule was sharp and revealed a typical capsule shape.[74]

Figure 8d shows that 700 nm IPLVVPL-PMAA hydrogel internalization by SK-OV-3 cells increases from 34 ± 5 to 76 ± 1% after 1 and 24 h incubation with the hydrogels, demonstrating 3.8- and 10-fold greater cell internalization than that observed for PC-3 (hepsin-negative) cells (5±3 and 20±7% for 1 and 24 hours of incubation, respectively). The comparison between MCF-7 (hepsin +) and PC-3 (hepsin -) cells shows that the cell internalization of the 700 nm peptide-modified hydrogels is 2.6- to 5.8-fold higher ($p<0.05$ for 3, 6 and 24 h) in the hepsin-positive MCF-7 cells. Therefore, 700 nm IPLVVPL-PMAA hydrogels exhibit a selective binding affinity and enhanced cellular uptake relying on the homing function of the peptide towards hepsin. In addition, statistical analysis indicated that the internalization of the peptide-modified hydrogels was higher in SK-OV-3 (hepsin +) than that in MCF-7 ($p<0.05$) cells after 1 to 6 h incubation which could be related to the cell type. Therefore, the enhancement in internalization of IPLVVPL-PMAA by SK-OV-3 (hepsin +) cells can be explained by the synergistic effect of the cell hepsin-expression level and cell growing rate. The SK-OV-3 cells were previously reported to have an augmented internalization of IPLVVPL-attached liposomes compared to MCF-7 cells.[11] In a relevant study, the cytotoxicity of the peptide-modified liposomes was found to be higher in SK-OV-3 than in MCF-7 cells.[75]

The above results demonstrate that cell association with peptide-conjugated PMAA hydrogels is cell specific, which is an important feature for active tumor targeting. On the other hand, the combination of negative surface charge, soft hydrogel morphology, and submicrometer size favor passive targeting ability. Moreover, these hydrogels should exhibit prolonged circulation in the blood due to minimized hydrogel-protein interactions,[47,48] which should enhance their passive accumulation in tumors via extravasation across interstitial gaps (~ 200 to 1200 nm)[76] between vascular endothelial cells in tumor tissues.

It is worth noting that an important effect of a protein corona on particle targeting ability *in vivo* is contingent depending on the protein type/concentration, particle physicochemical properties and a ligand type.[77] For example, affibody-modified particles showed enhanced targeting ability upon human serum albumin treatment while inhibition of specific targeting was observed for the same system after incubation with human serum.[78] The hyaluronic acid-based capsules with protein corona were shown to exhibit improved specific interactions with the receptor-overexpressing cells and decreased non-specific cellular

association.[79] In addition, several studies have demonstrated that small molecules, *e.g.* folic acid, lactose, and peptide-conjugated delivery systems retained their targeting capability to specific cancer cells in the presence of biological level of serum.[80,81,77] In our work, the peptide-modified hydrogels are hydrophilic and carry a negative surface charge which should help to decrease protein adsorption on the particles.[47] The peptide sequence used in this work has been also demonstrated to have an excellent targeting capability both *in vitro* and *in vivo* studies.[10,11] Therefore, a protein corona may have a negligible effect on the targeting ability of the system which will be further tested *in vivo* in our future work.

Conclusions

We developed a facile method to modify PMAA multilayer hydrogel particles with a hepsin-targeting peptide (IPLVVPL-PEG-Cys-Lys[FITC]) through a thiol-amine reaction for active tumor cell targeting. The IPLVVPL-PMAA hydrogel particles maintained their cubical shape in both hydrated and dry states, were stable against aggregation in serum, and showed dual pH/redox triggered release of doxorubicin. The surface wettability of IPLVVPL-PMAA hydrogel film was measured with a contact angle of $\theta=49 \pm 2°$, indicating its hydrophilic nature. We also found that the particle size had a crucial effect on internalization by MCF-7 cancer cells. The 2 μm peptide-free PMAA hydrogels were internalized more efficiently compared to the 700 nm PMAA particles. After peptide-attachment, the MCF-7 (hepsin-positive) cell internalization of 700 nm hydrogels was increased 2-fold within 3 – 24 h incubation, indicating that the targeting ligand modification could improve the internalization of 700 nm hydrogels by hepsin-positive cells. In contrast, 2 μm IPLVVPL-PMAA hydrogels had suppressed cell internalization compared to the peptide-free PMAA hydrogels. Finally, we found that the internalization of 700 nm IPLVVPL-PMAA hydrogels was cell specific. The peptide-modified PMAA hydrogels underwent from a 3- to 10-fold higher uptake by hepsin-overexpressing MCF-7 and SK-OV-3 cells as compared to hepsin-negative PC-3 cells. Accounting for soft hydrogel morphology, negative surface charge, tunable size, and a robust and simple accessibility to ligand conjugation, these PMAA multilayer hydrogel particles hold great potential to achieve both active and passive targeting ability for future *in vivo* tumor-targeting drug delivery.

ACKNOWLEDGEMENTS

This work was supported by NSF Career Award #1350370 (EK) and by NIAMS grant #1R01AR071157-01A1 (NY). We thank Dr. Robert Galemmo, Dr. Mudit Vaid, Dr. Fei Liu, Mr. Aaron Alford and Mr. Allen Mao for technical assistance. The UAB High Resolution Imaging Facility is also acknowledged for the use of SEM and CLSM.

REFERENCES

(1). Zhong Y; Meng F; Deng C; Zhong Z Ligand-directed active tumor-targeting polymeric nanoparticles for cancer chemotherapy. Biomacromolecules 2014, 15, 1955–1969. [PubMed: 24798476]

(2). Bareford LM; Swaan PW Endocytic Mechanisms for Targeted Drug Delivery. Adv. Drug Deliv. Rev 2007, 59, 748–758. [PubMed: 17659804]

(3). Muro S Challenges in Design and Characterization of Ligand-Targeted Drug Delivery Systems. J. Control. Release 2012, 164, 125–137. [PubMed: 22709588]

(4). Arabi L; Badiee A; Mosaffa F; Jaafari MR Targeting CD44 expressing cancer cells with anti-CD44 monoclonal antibody improves cellular uptake and antitumor efficacy of liposomal doxorubicin. J. Control. Release, 2015, 220, 275–286. [PubMed: 26518722]

(5). Zhou G; Latchoumanin O; Hebbard L; Duan W; Liddle C; George J; Qiao L Aptamers as targeting ligands and therapeutic molecules for overcoming drug resistance in cancers. Adv. Drug Deliv. Rev 2018, DOI: 10.1016/j.addr.2018.04.005

(6). Liu R; Li X; Xiao W; Lam KS Tumor-targeting peptides from combinatorial libraries. Adv. Drug Deliv. Rev 2017, 110, 13–37. [PubMed: 27210583]

(7). David A Peptide ligand-modified nanomedicines for targeting cells at the tumor microenvironment. Adv. Drug Deliv. Rev 2017, 119, 120–142. [PubMed: 28506743]

(8). Sugahara KN; Teesalu T; Karmali PP; Kotamraju VR; Agemy L; Greenwald DR; Ruoslahti E Coadministration of a tumor-penetrating peptide enhances the efficacy of cancer drugs. Science 2010, 328, 1031–1035. [PubMed: 20378772]

(9). Murray AS; Varela FA; List K Type II Transmembrane Serine Proteases as Potential Targets for Cancer Therapy. Biol. Chem 2016, 397, 815–826 [PubMed: 27078673]

(10). Kelly KA; Setlur SR; Ross R; Anbazhagan R; Waterman P; Rubin MA; Weissleder R Detection of Early Prostate Cancer Using a Hepsin-Targeted Imaging Agent. Cancer Res. 2008, 68, 2286–2291. [PubMed: 18381435]

(11). Kang MH; Park MJ; Yoo HJ; hyuk KY; Lee SG; Kim SR; Yeom DW; Kang MJ; Choi YW RIPL Peptide (IPLVVPLRRRRRRRRC)-Conjugated Liposomes for Enhanced Intracellular Drug Delivery to Hepsin-Expressing Cancer Cells. Eur. J. Pharm. Biopharm 2014, 87, 489–499. [PubMed: 24704199]

(12). Danhier F; Feron O; Préat V To Exploit the Tumor Microenvironment: Passive and Active Tumor Targeting of Nanocarriers for Anti-Cancer Drug Delivery. J. Control. Release 2010, 148, 135–146. [PubMed: 20797419]

(13). Blanco E; Shen H; Ferrari M Principles of Nanoparticle Design for Overcoming Biological Barriers to Drug Delivery. Nat. Biotechnol 2015, 33, 941–951. [PubMed: 26348965]

(14). He C; Hu Y; Yin L; Tang C; Yin C; Effects of Particle Size and Surface Charge on Cellular Uptake and Biodistribution of Polymeric Nanoparticles. Biomaterials 2010, 31, 3657–3666. [PubMed: 20138662]

(15). Maeda H; Bharate GY; Daruwalla J Polymeric Drugs for Efficient Tumor-Targeted Drug Delivery Based on EPR-Effect. Eur. J. Pharm. Biopharm 2009, 71, 409–419. [PubMed: 19070661]

(16). Lu F; Wu SH; Hung Y; Mou CY Size effect on cell uptake in well-suspended, uniform mesoporous silica nanoparticles. Small 2009, 5, 1408–1413. [PubMed: 19296554]

(17). Cabral H; Matsumoto Y; Mizuno K; Chen Q; Murakami M; Kimura M; Terada Y; Kano MR,; Miyazono K; Uesaka M; Nishiyama N; Kataoka K Accumulation of sub-100 nm polymeric micelles in poorly permeable tumours depends on size. Nat. Nanotechnol 2011, 6, 815–823. [PubMed: 22020122]

(18). Liu Y; Tan J; Thomas A; Ou-Yang D; Muzykantov VR The Shape of Things to Come: Importance of Design in Nanotechnology for Drug Delivery. Ther. Deliv 2012, 3, 181–194. [PubMed: 22834196]

(19). Young KD The Selective Value of Bacterial Shape. Microbiol. Mol. Biol. Rev 2006, 70, 660–703. [PubMed: 16959965]

(20). Fang J; Nakamura H; Maeda H The EPR Effect: Unique Features of Tumor Blood Vessels for Drug Delivery, Factors Involved, and Limitations and Augmentation of the Effect. Adv. Drug Deliv. Rev 2011, 63, 136–151. [PubMed: 20441782]

(21). Kolesnikova TA; Skirtach AG; Möhwald H Red Blood Cells and Polyelectrolyte Multilayer Capsules: Natural Carriers versus Polymer-Based Drug Delivery Vehicles. Expert Opin. Drug Deliv 2013, 10, 47–58. [PubMed: 23078091]

(22). Wang C; Sun X; Cheng L; Yin S; Yang G; Li Y; Liu Z Multifunctional Theranostic Red Blood Cells for Magnetic-Field-Enhanced in Vivo Combination Therapy of Cancer. Adv. Mater 2014, 26, 4794–4802. [PubMed: 24838472]

(23). Merkel TJ; Chen K; Jones SW; Pandya AA; Tian S; Napier ME; Zamboni WE; DeSimone JM The effect of particle size on the biodistribution of low-modulus hydrogel PRINT particles. J. Control. Release 2012, 162, 37–44. [PubMed: 22705460]

(24). Agarwal R; Singh V; Jurney P; Shi L; Sreenivasan SV; Roy K Mammalian Cells Preferentially Internalize Hydrogel Nanodiscs Over Nanorods and Use Shape-Specific Uptake Mechanisms. Proc. Natl. Acad. Sci. U.S.A 2013, 110, 17247–17252. [PubMed: 24101456]

(25). Anselmo AC; Mitragotri S Impact of particle elasticity on particle-based drug delivery systems. Adv. Drug Deliv. Rev 2017, 108, 51–67. [PubMed: 26806856]

(26). Anselmo AC; Zhang M; Kumar S, Vogus DR; Menegatti S; Helgeson ME; Mitragotri S Elasticity of nanoparticles influences their blood circulation, phagocytosis, endocytosis, and targeting. ACS nano 2015, 9, 3169–3177. [PubMed: 25715979]

(27). Merkel TJ; Jones SW; Herlihy KP; Kersey FR; Shields AR; Napier M; Luft JC; Wu H; Zamboni WC; Wang AZ; Bear JE; DeSimone JM Using mechanobiological mimicry of red blood cells to extend circulation times of hydrogel microparticles. Proc. Natl. Acad. Sci. U. S. A, 2011, 108, 586–591. [PubMed: 21220299]

(28). Guo P; Liu D; Subramanyam K; Wang B; Yang J; Huang J; Auguste DT; Moses M A Nanoparticle elasticity directs tumor uptake. Nat. Commun 2018, 9, 130. [PubMed: 29317633]

(29). Cortez C; Tomaskovic-Crook E; Johnston APR; Scott AM; Nice EC; Heath JK; Caruso F Influence of Size, Surface, Cell Line, and Kinetic Properties on the Specific Binding of A33 Antigen-Targeted Multilayered Particles and Capsules to Colorectal Cancer Cells. ACS Nano 2007, 1, 93–102. [PubMed: 19206525]

(30). Popov A; Popova N; Tarakina NV; Ivanova OS; Ermakov AM; Ivanov VK; Sukhorukov GB, Intracellular delivery of antioxidant CeO2 nanoparticles via polyelectrolyte microcapsules. ACS Biomaterials Science & Engineering 2018, 4, 2453–2462.

(31). Pavlukhina S; Sukhishvili S Polymer assemblies for controlled delivery of bioactive molecules from surfaces. Adv. Drug Deliv. Rev 2011, 63, 822–836. [PubMed: 21684313]

(32). Liu F; Kozlovskaya V; Zavgorodnya O; Martinez-Lopez C; Catledge S; Kharlampieva E Encapsulation of Anticancer Drug by Hydrogen-Bonded Multilayers of Tannic Acid. Soft Matter 2014, 10, 9237–9247. [PubMed: 25284271]

(33). Johnston AP; Kamphuis MM; Such GK; Scott AM; Nice EC; Heath JK; Caruso F Targeting cancer cells: controlling the binding and internalization of antibody-functionalized capsules. ACS Nano 2012, 6, 6667–6674. [PubMed: 22872125]

(34). Poon Z; Lee JB; Morton SW; Hammond PT Controlling in vivo stability and biodistribution in electrostatically assembled nanoparticles for systemic delivery. Nano Lett. 2011, 11, 2096–2103. [PubMed: 21524115]

(35). Hinton TM; Monaghan P; Green D; Kooijmans SA; Shi S; Breheney K; Tizard M; Nicolazzo JA; Zelikin AN; Wark K Biodistribution of polymer hydrogel capsules for the delivery of therapeutics. Acta Biomater. 2012, 8, 3251–3260. [PubMed: 22659177]

(36). Xue B; Kozlovskaya V; Kharlampieva E Shaped Stimuli-Responsive Hydrogel Particles: Syntheses, Properties and Biological Responses. J. Mater. Chem. B 2017, 5, 9–35. [PubMed: 32263432]

(37). An Z; Kavanoor K; Choy ML; Kaufman LJ Polyelectrolyte microcapsule interactions with cells in two-and three-dimensional culture. Colloids Surf. B Biointerfaces 2009, 70, 114–123. [PubMed: 19162453]

(38). Alexander JF; Kozlovskaya V; Chen J; Kuncewicz T; Kharlampieva E; Godin B Cubical shape enhances the interaction of layer-by-layer polymeric particles with breast cancer cells. Adv. Healthc. Mater 2015, 4, 2657–2666. [PubMed: 26424126]

(39). Chen J; Kozlovskaya V; Goins A; Campos-Gomez J; Saeed M; Kharlampieva E Biocompatible shaped particles from dried multilayer polymer capsules. Biomacromolecules 2013, 14, 3830–3841. [PubMed: 24063405]

(40). Shao J; Xuan M; Si T; Dai L; He Q Biointerfacing polymeric microcapsules for in vivo near-infrared light-triggered drug release. Nanoscale 2015, 7, 19092–19098. [PubMed: 26524005]

(41). Chen H; Di Y; Chen D; Madrid K; Zhang M; Tian C; Tang L; Gu Y Combined chemo-and photo-thermal therapy delivered by multifunctional theranostic gold nanorod-loaded microcapsules. Nanoscale 2015, 7, 8884–8897. [PubMed: 25913201]

(42). Xue B; Kozlovskaya V; Liu F; Chen J; Williams JF; Campos-Gomez J; Saeed M; Kharlampieva E Intracellular Degradable Hydrogel Cubes and Spheres for Anti-Cancer Drug Delivery. ACS Appl. Mater. Interfaces 2015, 7, 13633–13644. [PubMed: 26028158]

(43). Kozlovskaya V; Chen J; Tedjo C; Liang X; Campos-Gomez J; Oh J; Saeed M; Lungu CT; Kharlampieva E pH-Responsive Hydrogel Cubes for Release of Doxorubicin in Cancer Cells. J. Mater. Chem. B 2014, 2, 2494–2507. [PubMed: 32261419]

(44). Xue B; Wang W; Qin JJ; Nijampatnam B; Murugesan S; Kozlovskaya V; Zhang R; Velu SE; Kharlampieva E Highly Efficient Delivery of Potent Anticancer Iminoquinone Derivative by Multilayer Hydrogel Cubes. Acta biomater. 2017, 58, 386–398. [PubMed: 28583901]

(45). Kozlovskaya v.; Zavgorodnya O; Ankner j. F.; Kharlampieva E Controlling internal organization of multilayer poly(methacrylic acid) hydrogels with polymer molecular weight. Macromolecules 2015, 48, 8585–8593.

(46). Verma A; Stellacci F Effect of surface properties on nanoparticle–cell interactions. Small 2010, 6, 12–21. [PubMed: 19844908]

(47). Maeda H; Nakamura H; Fang J The EPR effect for macromolecular drug delivery to solid tumors: Improvement of tumor uptake, lowering of systemic toxicity, and distinct tumor imaging in vivo. Adv. Drug Deliv. Rev 2013, 65, 71–79. [PubMed: 23088862]

(48). Fröhlich E The role of surface charge in cellular uptake and cytotoxicity of medical nanoparticles. Int. J. Nanomedicine 2012, 7, 5577. [PubMed: 23144561]

(49). Kozlovskaya V; Kharlampieva E; Khanal BP; Manna P; Zubarev ER; Tsukruk VV Ultrathin Layer-by-Layer Hydrogels with Incorporated Gold Nanorods as pH-Sensitive Optical Materials. Chem. Mater 2008, 20, 7474–7485.

(50). Yuan Y; Lee TR In Surface Science Techniques; Bracco G, Holst B, Eds.; Springer: Berlin, 2013; p 3

(51). Vlierberghe SV; Dubruel P; Schacht E Biopolymer-Based Hydrogels as Scaffolds for Tissue Engineering Applications: A Review. Biomacromolecules 2011, 12, 1387–1408. [PubMed: 21388145]

(52). Pan YJ; Chen YY; Wang DR; Wei C; Guo J; Lu DR; Chu CC; Wang CC Redox/pH dual Stimuli-responsive Biodegradable Nanohydrogels with Varying Responses to Dithiothreitol and Glutathione for Controlled Drug Release. Biomaterials 2012, 33, 6570–6579. [PubMed: 22704845]

(53). Wang Z; Luo T; Sheng R; Li H; Sun J; Cao A Amphiphilic Diblock Terpolymer PMAgala-b-P (MAA-co-MAChol)s with Attached Galactose and Cholesterol Grafts and Their Intracellular pH-Responsive Doxorubicin Delivery. Biomacromolecules 2015, 17, 98–110. [PubMed: 26682643]

(54). Jin S; Wan J; Meng L; Huang X; Guo J; Liu L; Wang C Biodegradation and Toxicity of Protease/Redox/pH Stimuli-Responsive PEGlated PMAA Nanohydrogels for Targeting Drug Delivery. ACS Appl. Mater. Interfaces 2015, 7, 19843–19852. [PubMed: 26288386]

(55). Nel AE; Mädler L; Velegol D; Xia T; Hoek EMV; Somasundaran P; Klaessig F; Castranova V; Thompson M Understanding Biophysicochemical Interactions at the Nano–Bio Interface. Nat. Mater 2009, 8, 543–557. [PubMed: 19525947]

(56). Zelikin AN; Breheney K; Robert R; Tjipto E; Wark K Cytotoxicity and Internalization of Polymer Hydrogel Capsules by Mammalian Cells. Biomacromolecules 2010, 11, 2123–2129. [PubMed: 20614935]

(57). Wu W; Shen J; Banerjee P; Zhou S Chitosan-Based Responsive Hybrid Nanogels for Integration of Optical pH-Sensing, Tumor Cell Imaging and Controlled Drug Delivery. Biomaterials 2010, 31, 8371–8381. [PubMed: 20701965]

(58). She S; Xu C; Yin X; Tong W; Gao C Shape deformation and recovery of multilayer microcapsules after being squeezed through a microchannel. Langmuir 2012, 28, 5010–5016. [PubMed: 22381035]

(59). Ochs CJ; Such GK; Städler B; Caruso F Low-Fouling, Biofunctionalized, and Biodegradable Click Capsules. Biomacromolecules 2008, 9, 3389–3396. [PubMed: 18991459]

(60). Chen S; Li L; Zhao C; Zheng J Surface Hydration: Principles and Applications toward Low-Fouling/Nonfouling Biomaterials. Polymer 2010, 51, 5283–5293.

(61). Gratton SEA; Ropp PA; Pohlhaus PD; Luft JC; Madden VJ; Napier ME; DeSimone JM The Effect of Particle Design on Cellular Internalization Pathways. Proc. Natl. Acad. Sci. U.S.A 2008, 105, 11613–11618. [PubMed: 18697944]

(62). Costa RR; Girotti A; Santos M; Arias FJ; Mano JF; Rodríguez-Cabello JC Cellular Uptake of Multilayered Capsules Produced with Natural and Genetically Engineered Biomimetic Macromolecules. Acta Biomater. 2014, 10, 2653–2662. [PubMed: 24561713]

(63). Bishop NE An Update on Non-Clathrin-Coated Endocytosis. Rev. Med. Virol 1997, 7, 199–209. [PubMed: 10398484]

(64). Kastl L; Sasse D; Wulf V; Hartmann R; Mircheski J; Ranke C; Carregal-Romero S; Martínez-López JA; Fernández-Chacón R; Parak WJ; Elsasser HP; Rivera_Gil P Multiple Internalization Pathways of Polyelectrolyte Multilayer Capsules into Mammalian Cells. ACS Nano 2013, 7, 6605–6618. [PubMed: 23826767]

(65). Patiño T; Soriano J; Barrios L; Ibáñez E; Nogués C Surface modification of microparticles causes differential uptake responses in normal and tumoral human breast epithelial cells. Sci Rep 2015, 5, 11371. [PubMed: 26068810]

(66). Petros RA; DeSimone JM Strategies in the design of nanoparticles for therapeutic applications. Nat. Rev. Drug Discov 2010, 9, 615–627. [PubMed: 20616808]

(67). Oh N; Park JH (2014). Endocytosis and exocytosis of nanoparticles in mammalian cells. Int. J. Nanomedicine 2014, 9, 51–63. [PubMed: 24872703]

(68). Bareford LM; Swaan PW Endocytic Mechanisms for Targeted Drug Delivery. Adv. Drug Deliv. Rev 2007, 59, 748–758. [PubMed: 17659804]

(69). Zelikin AN; Breheney K; Robert R; Tjipto E; Wark K Cytotoxicity and Internalization of Polymer Hydrogel Capsules by Mammalian Cells. Biomacromolecules 2010, 11, 2123–2129. [PubMed: 20614935]

(70). Gratton SEA; Napier ME; Ropp PA; Tian S; DeSimone JM Microfabricated Particles for Engineered Drug Therapies: Elucidation into the Mechanisms of Cellular Internalization of PRINT Particles. Pharm. Res 2008, 25, 2845–2852. [PubMed: 18592353]

(71). Mintern JD; Percival C; Kamphuis MMJ; Chin WJ; Caruso F; Johnston APR Targeting Dendritic Cells: The Role of Specific Receptors in the Internalization of Polymer Capsules. Adv. Healthc. Mater 2013, 2, 940–944. [PubMed: 23335448]

(72). Reuter KG; Perry JL; Kim D; Luft JC; Liu R; DeSimone JM Targeted PRINT Hydrogels: The Role of Nanoparticle Size and Ligand Density on Cell Association, biodistribution, and Tumor Accumulation. Nano Lett. 2015, 15, 6371–6378. [PubMed: 26389971]

(73). Yuan H; Li J; Bao G; Zhang S Variable Nanoparticle-Cell Adhesion Strength Regulates Cellular Uptake. Phys. Rev. Lett 2010, 105, 138101. [PubMed: 21230813]

(74). Yan Y; Wang Y; Heath JK; Nice EC; Caruso F Cellular Association and Cargo Release of Redox-Responsive Polymer Capsules Mediated by Exofacial Thiols. Adv. Mater 2011, 23, 3916–3921. [PubMed: 21809395]

(75). Yoon HY; Kwak SS; Jang MH; Kang MH; Sung SW; Kim CH; Kim SR; Yeom DW; Kang MJ; Choi YW Docetaxel-loaded RIPL Peptide (IPLVVPLRRRRRRRRC)-conjugated Liposomes: Drug release, Cytotoxicity, and Antitumor Efficacy. Int. J. Pharm 2017, 523, 229–237. [PubMed: 28341149]

(76). Wong PT; Choi SK Mechanisms of drug release in nanotherapeutic delivery systems. Chem. Rev 2015, 115, 3388–3432. [PubMed: 25914945]

(77). Xiao W; Xiong J; zhang S; Xiong Y; Zhang H; Gao H Influence of ligands property and particle size of gold nanoparticles on the protein adsorption and corresponding targeting ability. Int. J. Pharm 2018, 538, 105–111. [PubMed: 29341915]

(78). Dai Q; Yan Y; Guo J; Björnmalm M; Cui J; Sun H; Caruso F Targeting Ability of Affibody-Functionalized Particles Is Enhanced by Albumin but Inhibited by Serum Coronas. ACS Macro Lett. 2015, 4, 1259–1263.

(79). Ju Yi.; Dai Q; Cui J; Dai Y; Suma T; Richardson JJ Caruso F Improving Targeting of Metal–Phenolic Capsules by the Presence of Protein Coronas. ACS Appl. Mater. Interfaces 2016, 8, 22914–22922. [PubMed: 27560314]

(80). Du C; Deng D; Shan L; Wan S; Cao J; Tian J; Achilefu S; Gu Y A pH-sensitive doxorubicin prodrug based on folate-conjugated BSA for tumor-targeted drug delivery. Biomaterials 2013, 34, 3087–3097. [PubMed: 23374705]

(81). Sun J; Jiang L; Lin Y; Gerhard EM; Jiang X; Li L; Yang J; Gu Z Enhanced anticancer efficacy of paclitaxel through multistage tumor-targeting liposomes modified with RGD and KLA peptides. Int. J. Nanomed 2017,12, 1517–1537.

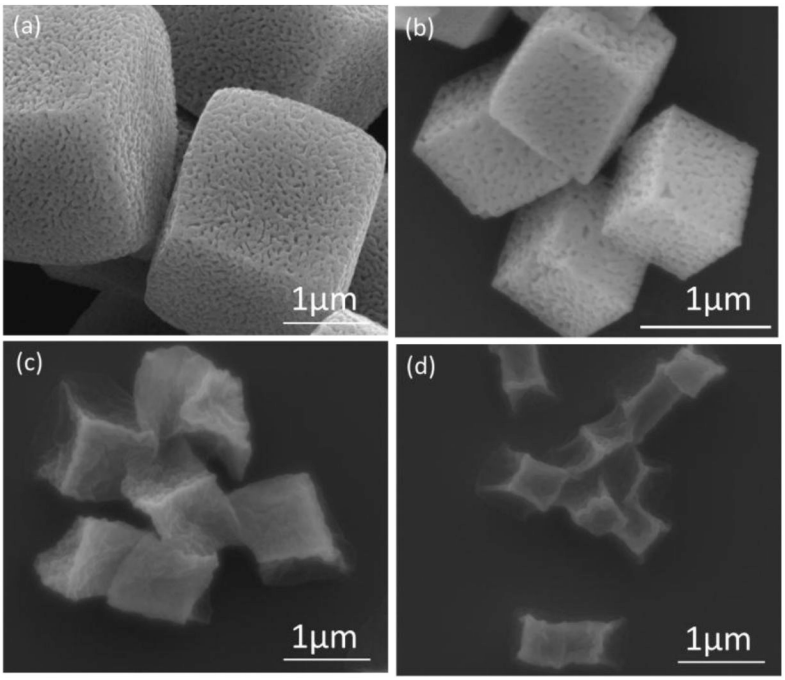

Figure 1.
SEM images of manganese oxide templates of (a) 2 μm and (b) 700 nm and their corresponding PMAA hydrogel cubes (c, d).

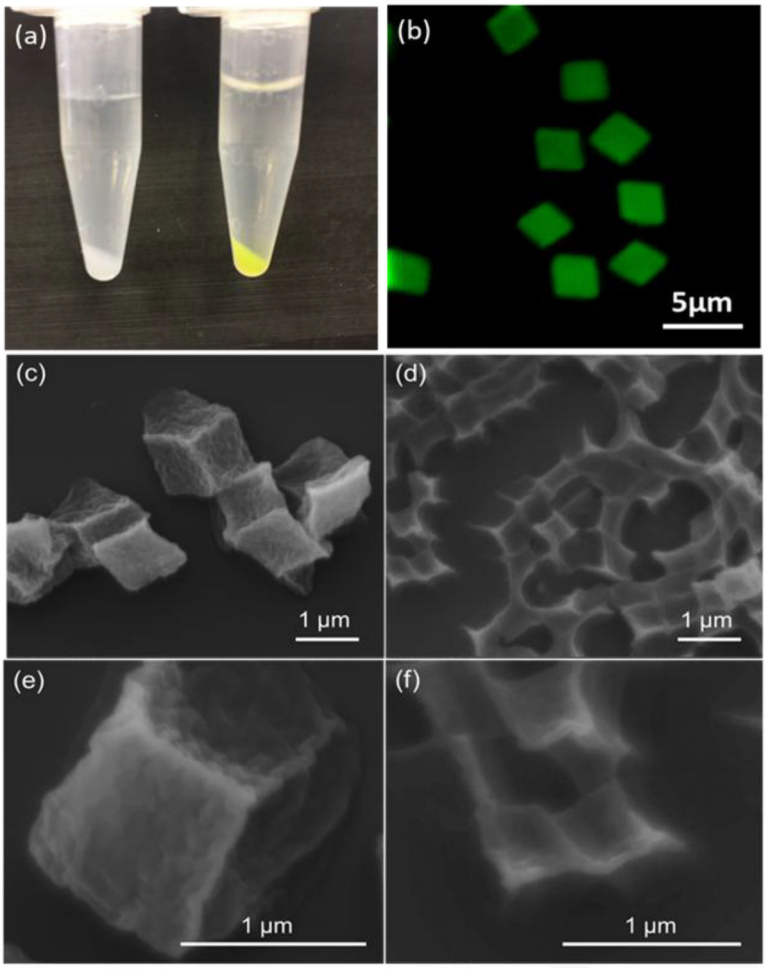

Figure 2.

(a) A photograph of 2-μm PMAA hydrogels before (left) and after (right) modification with the targeting peptide. (b) The CLSM image of 2-μm peptide-conjugated hydrogels (IPLVVPL-PMAA hydrogels) in solution at pH = 7.4. (c, d, e, f) SEM images of IPLVVPL-PMAA hydrogel cubes of (c, e) 2 μm and (d, f) 700 nm in diameter.

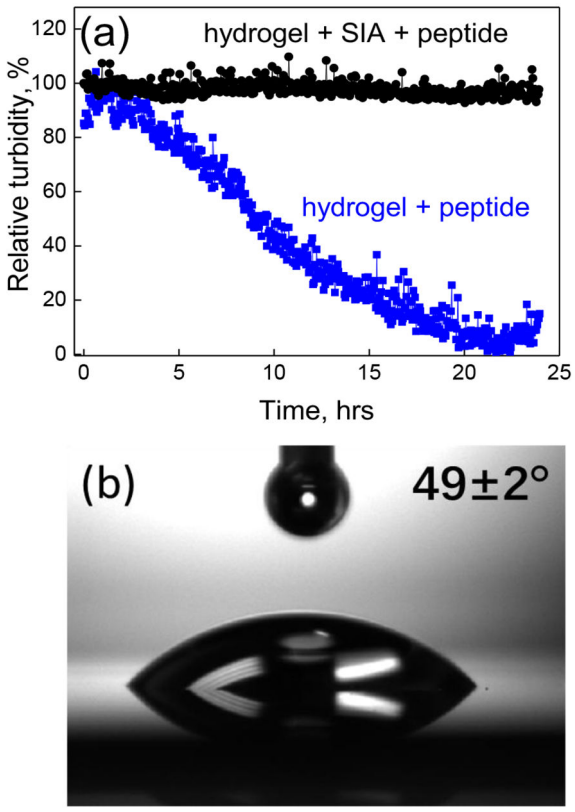

Figure 3.

(a) Relative turbidity measurements of 2-μm PMAA hydrogels after peptide conjugation as monitored using fluorometry (λ = 700 nm): the solution turbidity of SIA-treated (black circles) and untreated (blue squares) PMAA hydrogels in the presence of thiol-containing peptide molecules (0.15 mg mL^{-1} IPLVVPL-PEG-Cyc-Lys[FITC], pH = 6.8). (b) The optical image of a water drop placed on IPLVVPL-$(PMAA)_5$ hydrogel film.

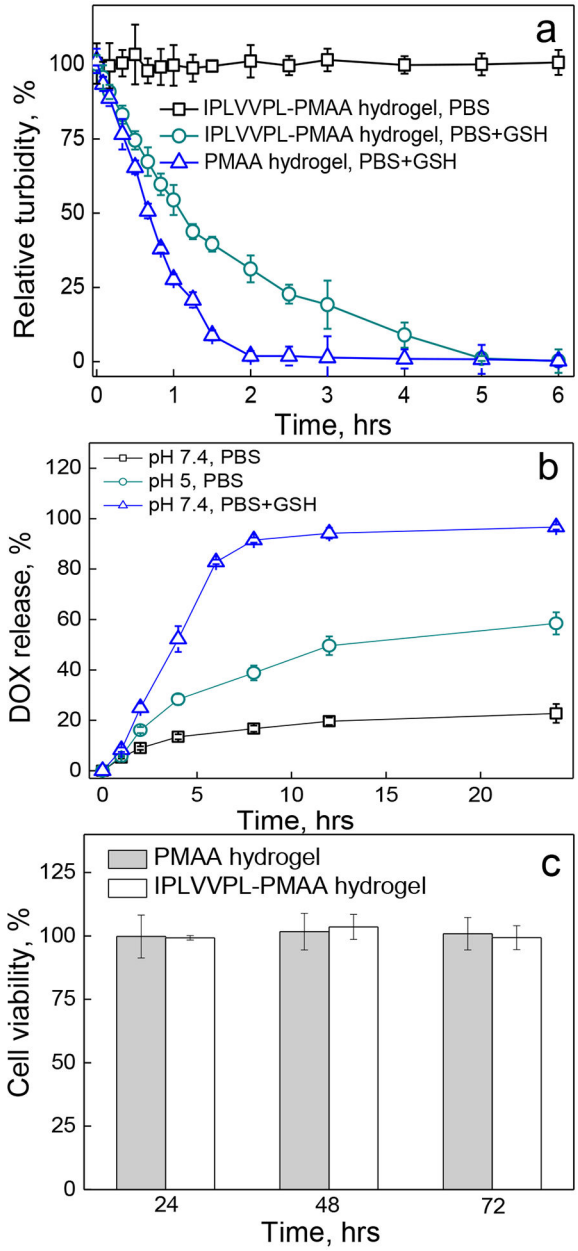

Figure 4.

(a) Relative turbidity (%) of 2 μm peptide-free PMAA (triangles) and IPLVVPL-PMAA hydrogel cubes (circles) after 6 h incubation in the presence of 5 mM GSH at pH=7.4 (PBS, 37 °C) as analyzed using fluorometry; the IPLVVPL-PMAA hydrogels incubated at pH=7.4 (PBS, 37 °C) were used as control (squares). (b) DOX release (%) from 2 μm DOX-loaded IPLVVPL-PMAA hydrogels at pH=7.4 (squares), at pH = 5 (circles), and at pH = 7.4 in the presence of 5 mM GSH (triangles) at 37 °C as analyzed by UV-vis spectroscopy. (c) Viability of MCF-7 cells after incubation with 2 μm peptide-free PMAA (light grey) and IPLVVPL-PMAA (white) hydrogels for 24, 48 and 72 h

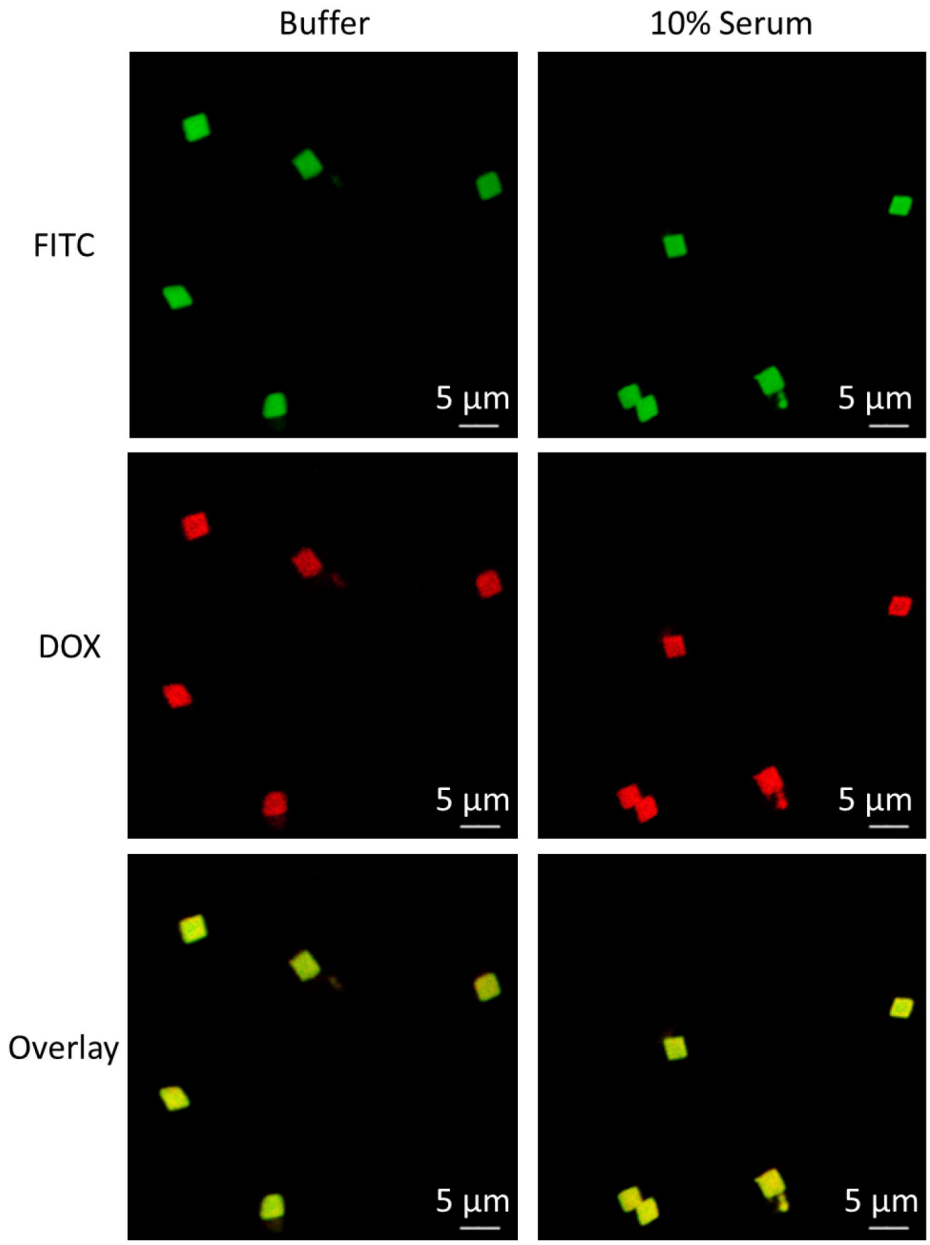

Figure 5.

Confocal images of DOX-loaded IPLVVPL-PMAA hydrogels after 24-h incubation at 37 °C in 0.01 M phosphate buffer at pH = 7.4 (left column) and in the presence of 10% serum in 0.01 M phosphate buffer at pH = 7.4 (right column).

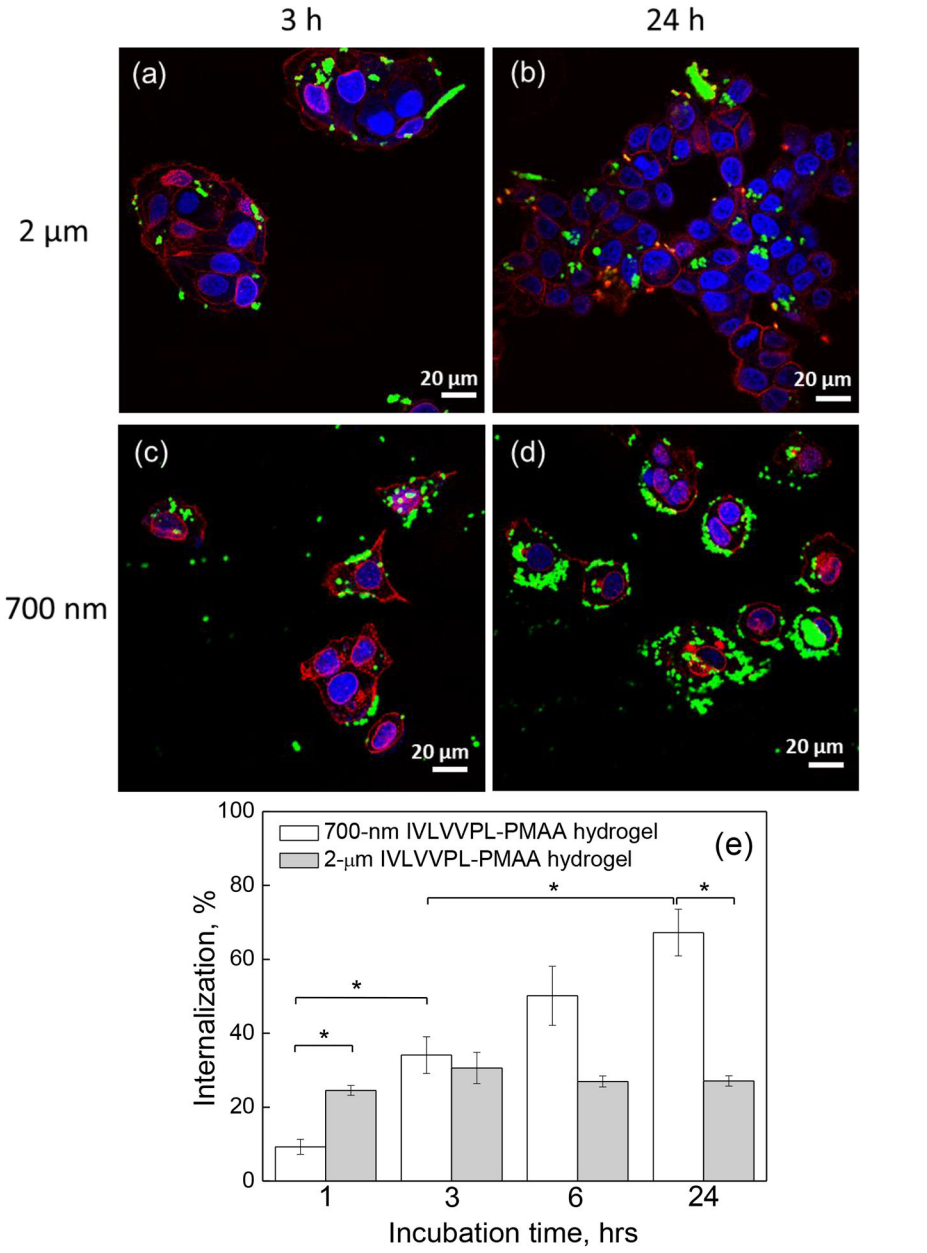

Figure 6.

CLSM images of MCF-7 cells after (a, b) 3 h and (c, d) 24 h incubation with (a, c) 2 μm or (b, d) 700 nm peptide-free PMAA hydrogels particles; The cell nuclei and membranes were stained with DAPI (blue) and Wheat Germ Agglutinin, Alexa Fluor™ 555 Conjugate (WGA Alexa 555) (red), respectively, while hydrogels emit green fluorescence (FITC). Scale bar is 20 μm in all images. (e) MCF-7 cell internalization (%) of 2 μm and 700 nm peptide-free PMAA hydrogels as measured by flow cytometry. (*:$p<0.05$, #:$p<0.01$; data is represented as mean ± sd, n=2–4)

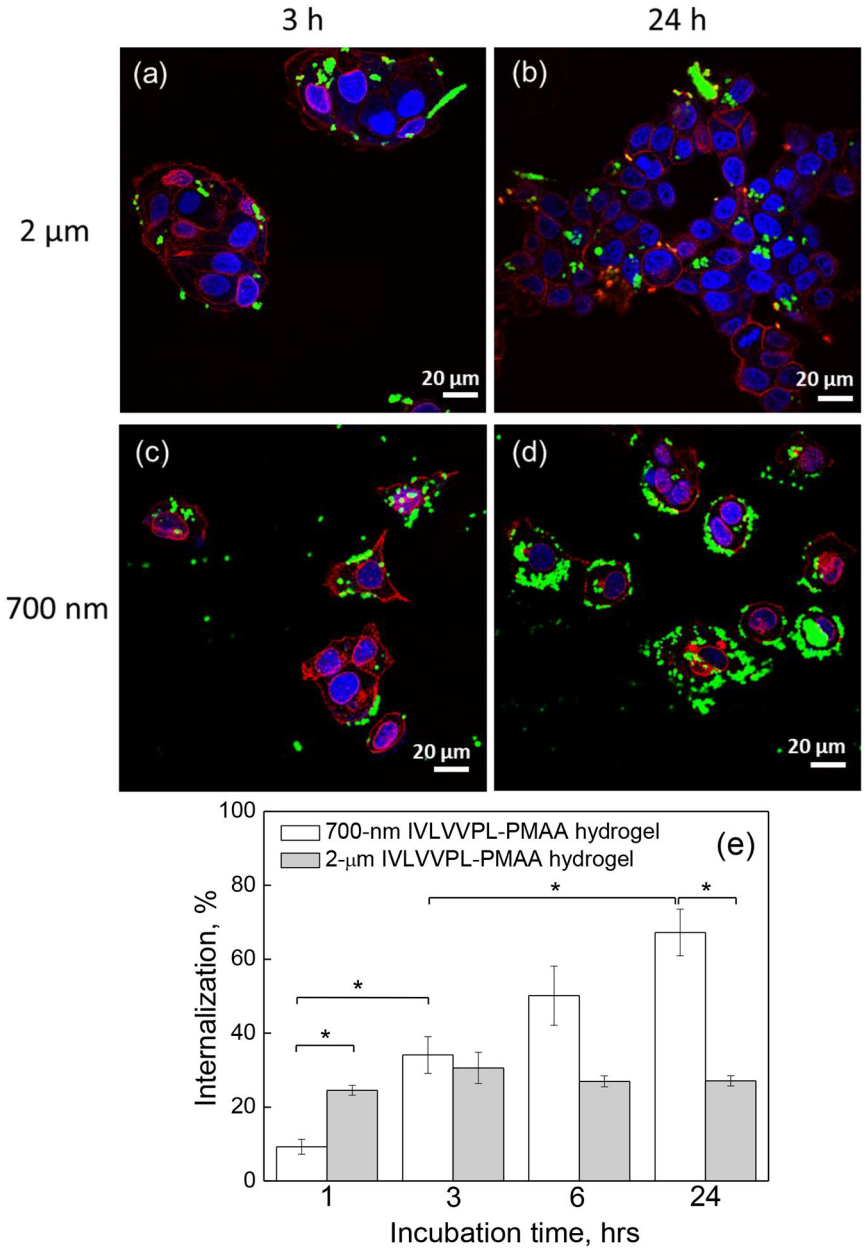

Figure 7.

CLSM images of MCF-7 cells after incubation with (a, b) 2 μm and (c, d) 700 nm IPLVVPL-PMAA hydrogels for (a, c) 3 h or (b, d) 24 h. The cell nuclei and membranes were stained with DAPI (blue) and Wheat Germ Agglutinin, Alexa Fluor™ 555 Conjugate (WGA Alexa 555) (red), respectively, while hydrogels emit green fluorescence (FITC). Scale bar is 20 μm in all images. (e) MCF-7 cell internalization (%) of 2 μm and 700 nm IPLVVPL-PMAA hydrogels as measured by flow cytometry (*:$p<0.05$; data is represented as mean ± sd, n=2).

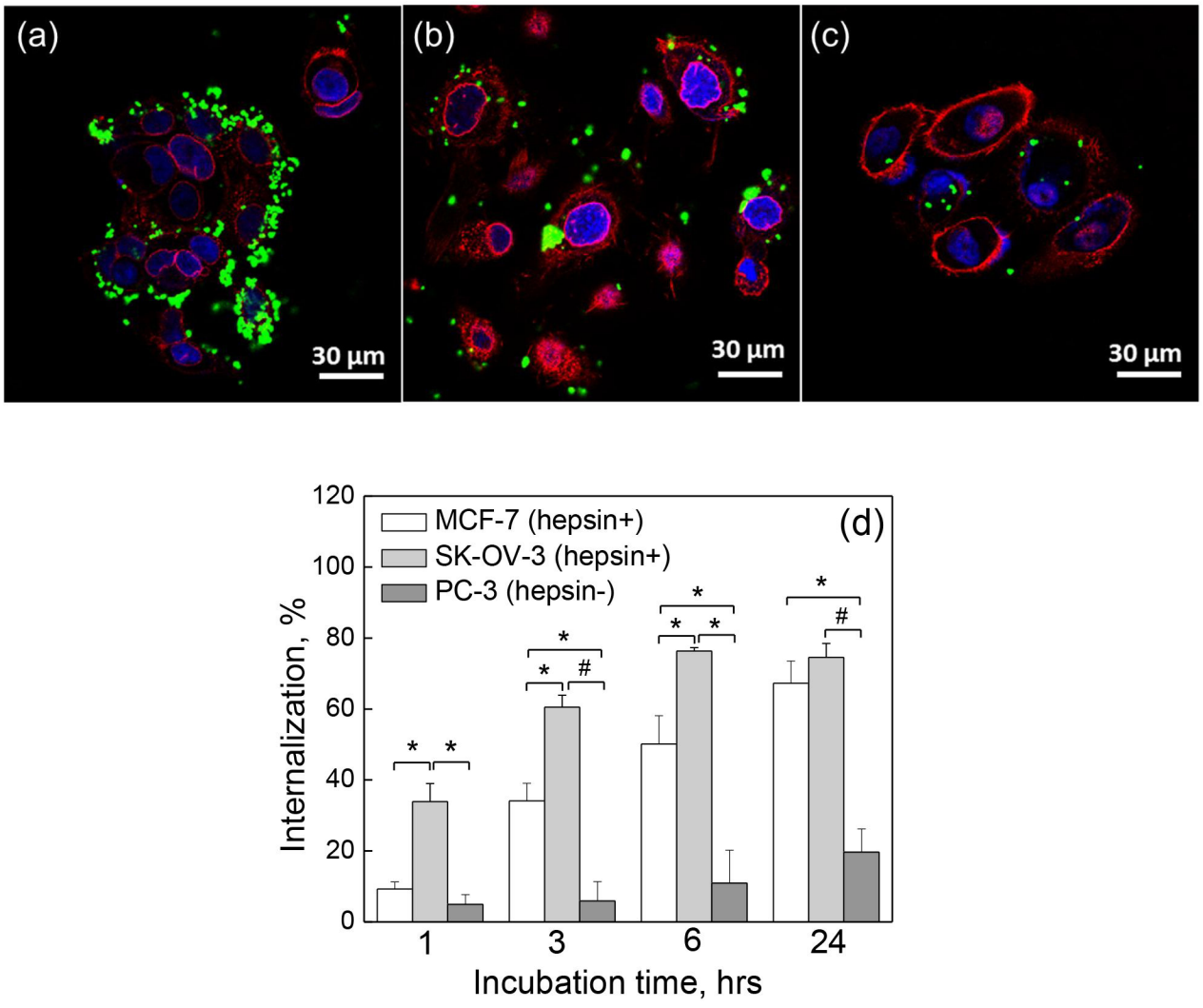

Figure 8.

CLSM images of (a) MCF-7, (b) SK-OV-3 and (c) PC-3 cells after 3 h incubation with 700 nm IPLVVPL-PMAA hydrogels. The cell nuclei and membranes were stained with DAPI (blue) and Wheat Germ Agglutinin, Alexa Fluor™ 555 Conjugate (WGA Alexa 555) (red), respectively, while hydrogels emit green fluorescence (FITC). Scale bar is 30 μm in all images. (d) Cell internalization (%) of 700 nm IPLVVPL-PMAA hydrogels by hepsin-positive (+) MCF-7 (white) and SK-OV-3 (light grey), and hepsin-negative (−) PC-3 (dark grey) cells as measured by flow cytometry (*$p<0.05$, $^{\#}p<0.01$; data is represented as mean ± sd, n=2).

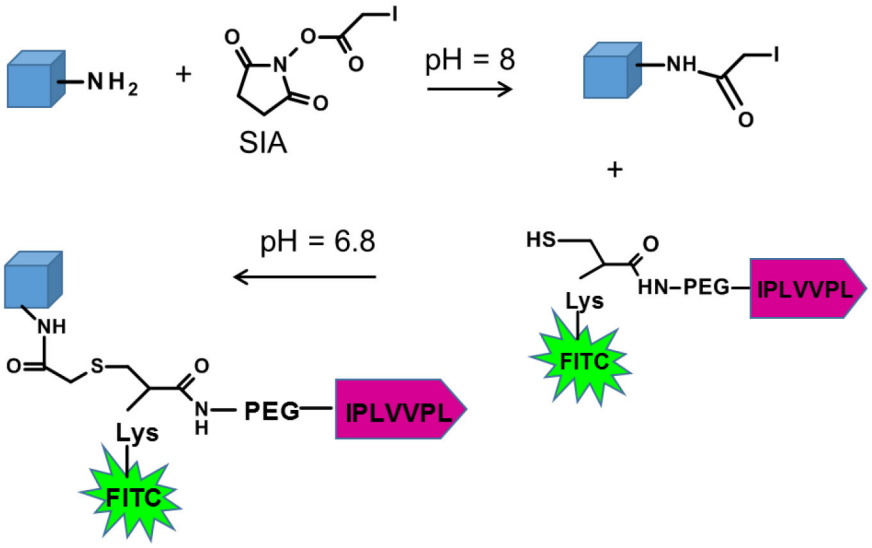

Scheme 1.

The peptide conjugation to PMAA hydrogels was carried out by reaction of amines on the hydrogel particles with succinimidyl iodoacetate (SIA) followed by linking of IPLVVPL via thiol conjugation. The Cys-Lys linker moiety carries the fluorescent marker, FITC.